SENSITIVITY OF THERMALLY DEPOSITED TITANIUM DIOXIDE THIN FILM FOR LIQUEFIED PETROLEUM GAS SENSING APPLICATION

BY

OSUMBAH PAUL OTIENO

A THESIS

SUBMITTED IN PARTIAL FULLFILMENT OF THE REQUIREMENTS FOR THE DEGREE OF MASTER OF SCIENCE IN EXPERIMENTAL PHYSICS

DEPARTMENT OF PHYSICS AND MATERIALS SCIENCE

MASENO UNIVERSITY

ABSTRACT

Titanium dioxide thin films have a wide scope of application including gas sensing. Other studies have been carried on the sensing ability of TiO_2 to natural gases (O_2, CO_2 and H_2) and hydrocarbons (ethanol and butane). This study investigated if thermally deposited TiO_2 thin film is sensitive to LPG by identifying thermal deposition conditions, assessing the variation in sheet resistivity of TiO_2 when exposed to LPG and correlating the sensitivity to the optical properties of the TiO_2 films. TiO_2 films were thermally deposited on microscope glass slides in a square pattern to allow for a four point probe using Van der Pauw setup to measure the sheet resistivity of the films using Keithley 2400 sourcemeter. The resistivity was mea sured in three phases; before, during and after exposure to LPG at room temperature. In all the samples tested, there was a decline in resistance between 0.009 kΩ and 0.04 kΩ when the film was exposed to LPG and about 90% recovery when withdrawn from the LPG rich environment. The change in sheet resistivity was used to deduce film sensitivity to LPG. The film's refractive index was obtained in the range of 1.67 to 1.88 at 550 nm wavelength from the transmittance spectra and used to calculate film porosity. The film thickness was measured using Alpha-step IQ (surface profilometer). The sensitivity of the film was observed to increase with increase in refractive index and decrease in film thickness and film porosity. The improved response of the thinner films over thicker films shows that conduction mainly occurs at the pore phase rather than at the solid phase. This study reveals that TiO_2 thin film is sensitive to LPG at room temperature and hence the material is viable for use in fabricating LPG sensors.

CHAPTER ONE

INTRODUCTION

1.0 Background Information

A sensor is a device which samples a phenomenon (electrical or non-electrical) and delivers a proportional output in terms of which the phenomenon may be measured or with which control action can be initiated [1]. Gas sensor systems are able to capture and process signals generated by specific and reproducible interaction with gas molecules. The development of this kind of devices has only been possible by the systematic production and characterization of new sensing materials. There are already commercial gas sensor devices used for identification of specific contaminants or common mixtures. However, much has yet to be done in order to improve sensitivity, selectivity, stability and production cost of these devices. Other practical concerns such as minimization of size, reduction of weight and lowering power consumption of gas sensors are major challenges. Oxide semiconductor films are promising for gas sensors applications due to the consistency of changes on their electrical conductivity upon interaction with environmental gases such as oxygen (O_2), carbon dioxide (CO_2) and hydrogen (H_2) [2].

Resistive metal oxide sensors have been used to measure a wide variety of physical and chemical properties and are among the most common and cheap sensors commercially available. There are, for example, photo-resistive sensors, which use materials that change conductivity with light absorption; thermo-resistive sensors in which resistivity variation is controlled by the temperature; piezo-resistive sensors, that use the change in resistance with mechanical stress; magneto-resistive sensors based on the resistivity

change in the presence of an external magnetic field and chemo-resistive that measure the resistivity change produced by the interaction of a chemical substance with the sensing material. The materials employed in these sensors are frequently produced in thin film form. In the gas sensor field, the most suitable materials for sensors of the chemo-resistive type are metal oxides [3].

Gas sensing technology research has been focused on solid state electronic sensors and electrochemical sensors due to their convenient sizes and output signals that can be easily monitored by a measuring instrument. The other sensing technologies like flame emission spectroscopy, mass spectroscopy, gas chromatography and infra red sensing have received less attention because they are expensive and require well experienced operators [4]. Solid state sensors offer a comparatively long life expectancy and do not consume or burn the gas being detected unlike the catalytic sensors. The former adsorb the gas onto the sensor surface, changing the resistance of the sensor material. When the gas dissipates the sensor returns to its original condition, and hence no sensor material is consumed in the process.

Solid state sensors consist of one or more metal oxides from the transition metals such as tin oxide (SnO_2), aluminium oxide (AlO_2), and titanium dioxide (TiO_2). The metal oxide sensors are versatile and have been reported to detect a wide variety of gases [2, 4, 5]. Different response characteristics are achieved by changing the semiconductor materials, processing techniques and sensor operating temperature.

TiO_2 also known as titanium (IV) oxide or titania, is the naturally occurring oxide of titanium. It is a transition metal oxide with physical and chemical properties such as high refractive index ($n > 2.4$), transparency in the visible region, photo-catalytic activity and chemical stability. The material is known to exist in an amorphous form and crystallizes in three distinct structures: two tetragonal phases, anatase and rutile, and a third orthorhombic phase, brookite [6]. Rutile is the most dense and thermodynamically the most stable phase. It is widely used for optical coatings, microelectronic applications and protective layers. Anatase has drawn much interest for its hydrophilic and its photocatalytic properties which have led to applications such as anti-fogging and self cleaning glass [7], gas and water purification devices and gas sensor devices. Anatase has a higher photoactivity than rutile and brookite and is irreversibly converted to rutile at high temperature. When deposited as a thin film, its refractive index and colour make it an excellent antireflective optical coating for dielectric mirrors. As an anti-reflecting coating TiO_2 film is widely used in heat mirrors. TiO_2 is the most widely used white pigment because of its brightness. It is used in common substances like white paint, toothpaste, sun lotion, soap and coloured food.

For gas sensing application TiO_2 can be deposited into thin films, as a single-layer or multilayer form using a variety of methods such as; reactive sputtering [8, 9], spray pyrolysis [2], screen printing [3], sol-gel method [10] and spin coating [11]. A wide variation in the electrical and physical properties exists due to the deposition methods and deposition parameters such as; vacuum pressure, rate of deposition and the oxidation state of the starting materials. The ability to deposit TiO_2 with varied structures is highly

desirable and practicable. Since the sensing property of TiO_2 film is based on surface interactions, the reducing or oxidizing species affect conductivity of the film [2, 11]. Preparation method of TiO_2 is fundamental to obtain properties suitable for gas-sensing applications such as structural stability, porosity and high surface to volume ratio in order to emphasize surface effects.

Concerns about outdoor air-pollution are wide spread. However, it is less known that serious health-related problems may emerge from the indoor environments where LPG is used as a source of energy such as industries and homes. Exposure to these compounds is known to cause reactions such as mucous irritation, neurotoxic effects such as fatigue, lethargy, headache and nonspecific reactions, for instance, chest sounds and asthma-like symptoms [12]. Precise air quality monitoring is of great importance in both indoor and outdoor environments. Monitoring requires sensors capable of sensitively and selectively detecting low concentrations of poisonous and explosive gases. Detection can be best fulfilled with simple, cheap and replaceable sensors, most preferably electronic or semiconductor type that can be easily integrated into the existing monitoring and ventilation systems [13].

LPG refers to a group of hydrocarbon-based gases derived from crude oil refining or natural gas fractionation. Propane and butane or mixtures of the two are its key constituents [14]. LPG is liquefied under moderate pressure (~800kPa) to facilitate transport and then vaporized for use as a heating or engine fuel and sometimes as a raw material in chemical industries. LPG is flammable and has potential to create hazard if

not handled safely. The gas is colourless and odourless though some odour (ethanethiol) is added to improve nasal detection. In gas form, LPG is twice as heavy as air and tends to accumulate at the lowest possible levels such as cellars, pits and drains. It is easily liquefied by pressure; taking about $^{1}/_{250}{}^{th}$ of its gaseous volume, which implies that a large amount of LPG can be stored in a small volume. LPG forms a flammable mixture with air in a concentration between 2% and 10%, the vapour arising from leakage may be ignited at some distance from the point of escape and the flame can travel back to the source of gas leakage. The vapour at high concentration can have anaesthetic effect and subsequently asphyxiate by diluting the available oxygen. Leak detection of this gas is a prime safety precaution, both industrially and in the domestic environment where the gas is bottled in small quantities.

1.1 Statement of the Problem

While most semiconducting oxide gas sensors use heaters to raise their sensitivity, TiO_2 surface is readily responsive to gases at ambient temperatures or in the presence of natural light as used in photocalytic and self-cleaning surfaces. TiO_2 sensors can offer low energy consumption and readily usable surfaces that may be integrated in other systems like smart windows, domestic and industrial architectural designs. LPG is used in many industrial and domestic applications, despite its potential dangers due to fire outbreaks when the gas leaks. To help increase safety in the homes and industries, it is necessary to detect harmful presence of LPG in the environment. This study seeks to explore the relationships between thermal deposition conditions and the sensitivity of TiO_2 thin films with application in gas sensing.

1.2 Objectives of the Study

The main objective of this study was to find out if TiO_2 thin films are sensitive to LPG through realization of the following specific objectives;

i. Identify factors that affect thermal deposition of TiO_2 thin films on glass substrates.

ii. Assess whether sheet resistivity of TiO_2 thin films is altered in the presence of LPG.

iii. Correlate TiO_2 gas sensitivity to the film's optical properties.

1.3 Justification of the Study

Semi-conducting metal oxide based thin films as gas-sensitive material has currently received much attention from researchers owing to the film's portability, simplicity, low cost, and reduced size. The oxide films exhibit a significant change in their sheet conductivity when a change in the ambient gas composition occurs, and this change in conductivity forms the basis for a new generation of gas detection. Despite existence of regulations that control the filling and distribution of LPG to consumers, illegal traders also distribute into the chain and provide substandard services making the buying of LPG be on a buyer beware terms. Titanium dioxide is a versatile material that relies on the surface activity with uses in solar cells, photo-catalytic layer for self cleaning and electro-chromic displays. The active surface application makes TiO_2 viable for gas sensing application.

This study is a response to concerns about fire outbreaks in homes and in commercial places as a result of LPG leakages. Attempts to monitor gas leakages to reduce accidents have not been successful. This failure to reduce accidents can be attributed to factors which include the society's ignorance of safety measures, inaccessibility of the existing gas leakage detectors and cost constraints.

1.4 Scope of the Study

The study was limited to TiO_2 thin film deposited by thermal evaporation. The analysis was done on the films when exposed in ambient air and when exposed to LPG. The measurements done were transmittance spectrum, XRF analysis and sheet resistivity.

CHAPTER TWO

LITERATURE REVIEW

2.0 Introduction

This chapter discusses studies carried out on thin film deposition techniques and applications of thin films in gas sensing. Thermal deposition and TiO_2 gas sensing has been reviewed in line with findings from other studies.

2.1 TiO_2 Thin film deposition techniques

Thin films can be deposited using varied methods categorized mainly as Physical Vapour Deposition (PVD) and Chemical Vapour Deposition (CVD). PVD is the most common technique used to deposit optical thin films for a large variety of applications. The technique requires the ability to convert a solid material into a vapour form and to transport it to a surface onto which the film is to be deposited. Sputtering and evaporation in a vacuum are the prevalent techniques used in PVD. In PVD the atoms are controllably transferred from a source to a substrate where film formation and growth proceeds atomistically [9, 15].

In CVD a fluid precursor undergoes a chemical change at a solid surface leaving a non-volatile solid layer on the surface. The volatile compounds of a material to be deposited in CVD are introduced into the reaction chamber and are allowed to react producing a solid film on the substrate. Examples of CVD methods include, spray pyrolysis, sol-gel deposition, metal oxide chemical deposition and plasma enhanced chemical vapour deposition [3].

2.1.1 Spray pyrolysis

Pyrolysis refers to the thermal deposition of gaseous species of the required material to a wafer at a raised temperature. In the experiment done by Obida *et al* [2], TiO_2 film was deposited on glass substrates from 0.8 M solution of chemically pure $TiCl_4$ dissolved in ethanol. Filtered air was used as a carrier with a solution and gas flow rates of 0.7 ml/hr and 25 l/hr respectively. The substrate temperature range was 325 – 475°C and a spray time range of 5 – 30 minutes was used. Nanosized TiO_2 films with only anatase phase were produced. Castillo *et al* [16] used ultrasonic spray pyrolysis of titanium diisopropoxide to deposit TiO_2 thin films on fused quartz and silicon substrates. There was no crystallization observed on films deposited at temperatures below 400°C showing that anatase phase was linked only to the substrate temperature and not on critical thickness.

2.1.2 Sol-gel deposition

Two main sol-gel techniques have been used to produce thin films namely dip coating and spin coating. In dip coating the substrate is lowered into the solution and withdrawn at a suitable speed while in spin coating the solution is splashed onto a rotating substrate at a high speed. Sathyamoorthy *et al* [10] prepared TiO_2 thin films from titanium (IV) isopropoxide, deionized water, ethanol and hydrochloric using dip coating onto quartz substrates and annealing at various temperatures in air, structural transformation from amorphous to crystalline was observed. Comparable results were obtained by Ray *et al* [17], Mechiakh and Bensaha [18], Kozlowska *et al* [19] and Toan *et al* [30] with

variations on the source material composition and rate of withdrawal from the solutions. All the samples were annealed after deposition to crystallize.

Spin coating has been used by Mabrook and Hawkins [11] to prepare TiO_2 films on glass substrates by mixing 0.25 mg of TiO_2 powder in 2 ml solution of nitrogen-dimethylacetamide. The thickness of the film was adjusted by varying the concentration of the polymer, the speed of the spin and the coating time. Dang *et al* [4] used spin-coating to deposit TiO_2 films by varying the spin-coating speed (1000-8000 rpm) to obtain different film thicknesses. A stable anatase phase was exhibited in all the films.

2.1.3 Other CVD methods

Bernadi *et al* [20] used metal oxide chemical vapour deposition (MOCVD), titanium isopropoxide was heated onto glass and silicon substrates. The film thickness increased with deposition time. Plasma enhanced chemical vapour deposition (PECVD) has been used by Kozlowalska [19]. Screen printing has also been used by Trimboli [3].

2.1.4 Sputtering

Sputtering is a popular vacuum process used to deposit thin films for a wide variety of commercial and scientific uses. Sputtering methods are classified according to the type of discharge which generates the plasma in addition to the arrangement of the target and the substrate. The discharge types used commonly are the diode types (operated by direct current (DC) or radio frequency (RF)) and the magnetron types (either DC or RF). In magnetron sputtering, a permanent magnet is placed behind the target to form a toroidal-

type magnetic tunnel in which electrons are trapped and follow cycloidal motion close to the target which increases the plasma density [15].

Using radio frequency (RF) reactive sputtering, Dutta *et al* [21] deposited TiO_2 films on polycrystalline alumina substrates using Ti target in an Ar + O_2 mixture which resulted in. Films of different thicknesses (24 – 1000 nm) by varying sputter time. Dense films were produced with rutile structure when the substrates were annealed at 620°C. Dakka *et al* [22] sputtered TiO_2 films from TiO_2 target in Ar + O_2 environment and obtained amorphous films for different targets (new target, used target and used target with O_2. Hassan *et al* [23] obtained anatese films by RF magnetron sputtering of Ti target on unheated glass slides.

By direct current (DC) reactive magnetron sputtering, Karunagaran *et al* [24] deposited TiO_2 films on glass substrate using pure Ti target in Ar + O_2 gases and obtained amorphous films. Zhou *et al* [25] used the same method as Karunagaran to deposit TiO_2 on silicon substrates but altered the sputtering pressure to obtain rutile films at 0.3 Pa, anatase at 3.6 Pa and amorphous films at 1.2 Pa. These results were attributed to difference in the packing densities of the films created. Waita *et al* [26] used reactive magnetron sputtering to deposit TiO_2 films on glass substrates and obtained amorphous films whose crystallinity and stoichiometry was improved by annealing in air at 450°C. DC magnetron sputtering has been used in other studies [27].

2.1.5 Thermal evaporation

Among physical vapour deposition techniques, thermal evaporation (TE) is the one with the longest standing tradition, only being improved with advances in technology. In TE the source material is converted to vapour and transported in a high vacuum of about 10^{-6} mbar background pressure for deposition on to substrate. The high vacuum allows the vapour to reach the substrate without reacting or being scattered by other gas-phase atoms in the chamber and it increases the evaporated particle mean free path. The general TE set up is shown in Fig 2.1.

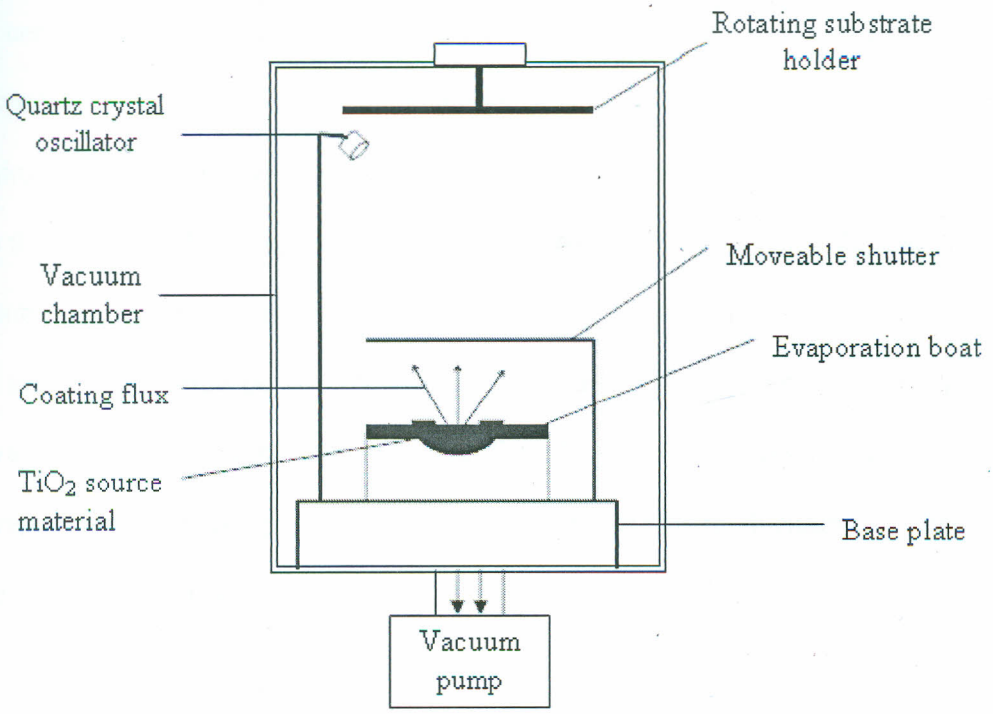

Fig 2.1: Thermal evaporation set-up

Brien *et al* [28], by thermal evaporation deposited Ti-Ni-Zr films on glass substrates using tungsten filaments. Nanocrystallized films were observed in all the films deposited at varied substrate temperatures. Chong *et al* [29] deposited TiO_2 thin films on unheated Si substrates from Ti with O_2 flow rate of 5000 sccm into the deposition chamber. The result showed that thermally oxidised Ti transformed to rutile phase at longer oxidation time or at higher oxidation temperature.

TE is a non-directional deposition method, the substrate-source material distance can be made large and still a high uniformity of the deposited film is achieved. This uniformity is certainly one of the advantages of TE over other methods that results in a high volume deposition rate. However, the fact that a lot of material is deposited all over the chamber brings in the problem of contamination and flaking since all components directly exposed to the vapour will be coated. Comparatively evaporation has a higher deposition rate than sputtering, with low atom energy (~0.1 eV), the substrate surface suffers less damage and is not heated during deposition. However it is difficult to control alloy composition in evaporation than in other methods. The film thickness too is limited to the size of the evaporation boat as opposed to the other methods where thickness is controlled by deposition time [15].

Varied deposition techniques have been used to coat TiO_2 films on different substrates revealing different characteristics in each study. The crystallinity or non-crystallinity of the films and film thickness are some of the issues arising out of variation in deposition

methods. Not much literature is available on thermal evaporation method as used on TiO_2 thin films and hence a need to fill in the gap for comparison with the other methods.

2.2 Types of gas sensors

Solid state semiconductor (SSS) sensors consist of a bead of tin oxide formed around two fine coils of platinum wire. When the bead is heated using one of the coils, the analyte gas will oxidize on the bead surface, changing the electrical conductivity as measured between the heated and unheated coils. Nearly all oxidizable gases can be detected on the SSS sensor. Selectivity is poor, but it can be modified slightly by changing the operating temperature and by doping the tin oxide with various elements. SSS sensors are inexpensive, but the sensitivity is not good (20-100 ppm) [13].

Combustible Gas Sensor consists of a coil of platinum wire which is electrically heated. When gases combust on the surface, some of the heat of combustion is transferred to the wire coil. The increase in coil temperature is reflected as an increase in electrical resistance.

2.2.1 Semiconducting oxide gas sensors

The most significant contribution in the development of semiconductive sensors was provided by Japanese scientists and engineers in 1968. Naayoshi Taguchi developed a series of ceramic sensors called Taguchi Gas Sensors (TGS) [30]. The operation principle of the "classical", Taguchi-type of semiconductor gas sensors is based on the change of the sensor resistance as the gas to be detected is simply adsorbed onto the sensor surface,

changing the resistance of the sensor material. When the gas is removed, the semiconductor returns to its original condition. No sensor material is consumed in the process, and hence the solid-state sensors offer a long life expectancy. This type of sensors represents a low-cost option to the standardized and bulky methods (for instance, gas chromatography or mass spectroscopy). Numerous materials that are to be usable as metal oxide sensors include single component oxides like TiO_2 [4], SnO_2 [4, 5, 31] and multi-component oxides such as $CaTiO_3$ [32] and ZnO doped TiO_2 [33]. Among the organic materials the phthalocyanines are the most used. There is on-going research in improving the sensor performance including sensitivity and most importantly, the chemical selectivity of these kinds of sensors [34].

Gases such as CO, H_2, and hydrocarbons can be oxidized by reaction with a metal oxide surface. If the oxygen equivalents in this reduction process arise due to chemisorbed species on the oxide, then the electrons released upon oxidation can alter the resistance of the oxide which forms the basis for gas sensing using semi-conducting oxides, such as SnO_2 and TiO_2 [2].

Metal oxide semiconductors are mainly used to detect small concentrations of reducing and combustible gases in air. Using SnO_2 thin films, Dang *et al* [4] observed a decrease in sheet resistance of the film when exposed to CO and CH_4 with a recovery time of less than 2 minutes. Response time and sensitivity improved with increase in operating temperature. Similar results were obtained by Licznerski [5]. Comini [31] observed that SnO_2 nanotubes were sensitive to NO_2 and CO by analysing isothermal response of

current flowing through the nanotubes at 400°C. LPG sensing was studied by Toan [32] using nano-crystalline perovskite oxide. The sensitivity of the films was observed to increase with the sensor voltage and was highest at 2.5 V. The recovery time was shortest at higher voltage (2.4 V). In a majority of the devices the detection mechanism of these gases requires oxygen in the atmosphere and is influenced by the presence of water vapour. It may also be observed that with increasing layer temperature, sensitivity reaches a maximum value and then fall towards zero, at higher temperatures. Since the optimum temperature depends on the gas compound, the operating temperature may be used as a means to change the selectivity of the device as observed by Comini [31].

2.2.2 TiO_2 thin film for gas sensing

While TiO_2 is not used as much as its low temperature analogue SnO_2, both materials are semiconducting metal oxides, whose defect structure and Schottky barrier formation have led them to possess similar operating principles. Titania sensors have been used to detect a wide variety of gaseous species. Obida *et al* [2] analysed the response of TiO_2 thin film to O_2, H_2 and CO. There was a drop in sheet resistivity of the films upon exposure to H_2 and CO, but for O_2 the sheet resistivity increased. The result indicated the behaviour of TiO_2 as an n-type semiconductor. The O_2 molecules adsorbed at the surface and at the grain boundaries extract electrons from the conduction band thus reducing concentration of the electrons and allow an increase in film resistivity. However, when a reducing gas comes into contact with the metal oxide surface, it reacts with the oxygen in the natural air. The combustion products (CO_2 and H_2O) depart and the electrons formerly trapped on the surface are returned to the metal oxide thereby increasing conductivity. A similar

explanation was put forth by Shobi [35]. The reversible decrease in resistivity with increase in temperature was attributed to evolution of adsorbed O_2 at film surface and grain boundaries.

Dang *et al* [4] observed an improvement in response time with increasing operating temperature for TiO_2 response to CO and CH_4 which was attributed to structural changes in the thin films. Dutta *et al* [21] observed that 240 nm thick TiO_2 films had the highest response compared to 120 nm and 170 nm films. The heightened sensitivity is attributed to grain size and depended on thickness of the film. The film is hypothesized to have had a switch from a depleted to a partly depleted sensor upon reaction of CO with the surface leading to higher sensitivity. The sensitivity was also attributed to surface roughness which resulted in increased gas adsorption.

Hydrocarbon sensing using TiO_2 thin films has received considerable attention; Kozlowska *et al* [19] observed a drop in current intensity of titania layer upon exposure to hexane, hexanol cyclohexane and benzene vapours at varied temperatures which was explained by the fact that TiO_2 layer is an n-type semiconductor. Sensor response was highest at 270°C for hexanol, 360°C for benzene and 440°C for cyclohexane, this was a positive solution to the problem of selectivity of TiO_2 sensor. However this study revealed weaknesses on the electrical stability of the film as observed in the change in the base line from 6.3 nA to 4.0 nA.

Trimboli [3] observed a drop in resistance when TiO_2 film was exposed to CO and propane. TiO_2 film response to ethanol, methanol and propanol have been studied by Ferrari *et al* [36], while Mabrook and Hawkins [11] found that TiO_2 is sensitive to Benzene at room temperature. All the films of thicknesses 5 μm, 10 μm, 15 μm and 20 μm had similar response to benzene but thinner films were more sensitive and had a more linear response. The result was attributed to the fact that the benzene molecules interacted with the holes by injecting electrons into the valence band. The injected electrons combine with holes, thus reducing the number of charge carriers and increase the resistance of the film. The TiO_2 thin films are sensitive to benzene at room temperature.

Several studies are available on sensitivity of TiO_2 thin films to hydrocarbons and other natural gases, however LPG sensing has largely been ignored despite its widespread usage both for domestic and commercial applications. Investigation of TiO_2 thin films deposited by thermal evaporation for LPG sensing shall offer some insight to fill in the gap observed in these studies.

CHAPTER THREE

BACKGROUND THEORY

3.0 Introduction

In this section the characteristics LPG and TiO_2 have been discussed. The general gas sensing mechanisms are highlighted with special attention to the use of electrical characterization to analyze the surface interaction with a sensed gas and estimation of film sensitivity to the sensed gas. The film composition analysis through X-ray fluorescence (XRF) has been discussed alongside thin film optics as used in calculating the refractive index and film porosity.

3.1 Liquefied Petroleum Gas (LPG)

LPG is a by-product of petroleum refining and is highly flammable. It is a dangerous fire and explosive hazard commercially available as propane (often found in colder climates), butane (higher freezing and boiling points) and butane-propane mixtures. Other synonyms used for LPG are; petroleum gas, bottled gas, n-propane. The molecular formula of propane is C_3H_8 and a structural formula of CH_3-CH_2-CH_3, butane chemical formula is C_4H_{10} and a structural formula of CH_3-CH_2-CH_2-CH_3 [6].

LPGs are widely used as fuel and as feedstock in chemical processes, automotive fuel and as propellants in pressurized aerosol containers. In some countries, propane, a natural gas is used as fuel gas in the household, industry, and vehicles. In organic synthesis it is used as an intermediate in petrochemical manufacture, a refrigerant and aerosol

propellant. Butane on the other hand is used in liquid fuels of high octane, organic synthesis of different chemicals and production of synthetic rubbers.

The industrial energy sector in Kenya is dominated by petroleum and electricity as the prime movers of the modern sector of the economy, but at domestic level, wood fuel and other biomass account for 68% of the total primary energy consumption, followed by petroleum at 22%, electricity at 9% and others at about 1% [14]. Regulatory function in petroleum sector is shared amongst various players, including Ministry of Energy and local authority. The private sector dominates the distribution network of petroleum products after the liberalization of the industry in 1994. Kenyan demand for LPG is estimated at 60,000 metric tonnes annually, which is supplied through direct importation and by the oil refinery in Mombasa [14]. All in all, LPG plays an important role in providing clean energy to the community and despite good safety promotions running through from production and packaging to consumption level [14], accidental leakage of LPG has caused a lot of injury and destruction of property

3.1.1 Hazards of LPG and its constituents

Cases of death following accidental or intentional inhalation of LPG have been reported. Patients complain of nausea, malaise, generalized weakness of the lower limbs and acute hepatitis that have been attributed to working in an enclosed space fixing gas cylinders containing a propane-butane mixture. Abnormal liver function and neurological symptoms have been found in patients after inhaling a mixture containing propane,

butane, and 2-methylpropane (30-35%). At very high levels, propane is a central nervous system (CNS) depressant and has asphyxiating properties [12].

In humans, absorption of butane is about 30-45% of the dose inhaled. Although there is no data on absorption through the skin, dermal penetration of butane is expected to be low since skin contact is transient due to the volatility of the compound. Reports have indicated abuse of LPG as an inhalant from lighters or hair/ deodorant sprays by teenagers and adolescents [12]. Butane abuse is fatal, arising mostly due to heart failure or multiple organ failure involving the central nervous system (CNS), cardiovascular system, pulmonary system and the liver. Butane induces severe acute neurological (seizure, somnolence, coma) or cardiovascular complications and minor symptoms such as nausea, dizziness, vomiting, headache, and sore throat [14]. The energy regulatory commission (ERC) – Kenya defines and regulates the use of LPG in Kenya by monitoring importation, transport and sale of LPG to consumers [37].

3.2 Gas Sensors

Classification of sensors is a difficult task. Some common classification schemes group the sensors by the applications, the input stimuli, (looking at what they measure), the conversion mechanisms, the materials used, the production technologies or the sensors characteristics such as cost, accuracy or range. Each of these approaches may be helpful in different sensor development stages.

According to the form of energy that generates the stimulus, the sensors can be divided into seven classes: mechanical, thermal, electrical, magnetic, optical, radiation or chemical. Mechanical sensors may be used to measure length, acceleration, flow, force, pressure or acoustic wave amplitude. Thermal sensors are used to measure temperature, specific heat, heat flow or entropy. Electrical sensors are used, for example, to measure charge, current, voltage, resistance, inductance or capacitance. Magnetic sensors are used to measure magnetic field intensity, magnetic flux density, magnetic moment or magnetic permeability. Optical sensors, sometimes also called radiant sensors, may be used to measure light properties, such as, intensity, phase, wavelength or polarization; or optical properties of a material, such as, emissivity or reflectivity. Finally, chemical sensors are used to determine chemical properties of substances, such as the composition of a mixture, the concentration of a substance, the pH or the rate of a chemical reaction [9, 38]. Gas sensors are obviously included in the chemical sensors' class.

3.2.1 Gas sensing methods

A set up that not only evaluates the gas sensing response but also reproduces as much as possible a real environment for a working gas sensor should be developed taking into consideration the varying atmospheric compositions, the electrical measurements and sample's varied operating temperature [9]. There are two main methods of producing a mixture of gases (varying atmospheric composition) namely; Static Volumetric Methods (SVM) and Dynamic Volumetric Methods (DVM).

SVM use a closed container where different compounds of the mixture are introduced sequentially. They are mainly used to build u p a mixture reserve by storage under pressure. However, they have a shortfall when it comes to sensitivity tests and evaluation of the sensor recovery. In DVM, a given flow rate of a gas is introduced onto the sensor in a test chamber with a known volume. The main dynamic technique used include; volumetric pumps, sonic orifices, mass flow controllers, diffusion and permeation controllers [9]. Electrically actuated valves controlled by a computer are used to control the gas flow and determine the concentration of the analyzed gas. The units used to express the concentration may vary from parts per million (ppm – number of particles of a contaminant per total number of particles in a mixture) units to flow rate measurements in standard cubic centimeter (sccm).

3.3 Gas Sensor Characterization

Sensors' characteristics can generally be grouped into static or dynamic parameters, environmental conditions and structural related characteristics. Static parameters describe the transfer function of a sensor, that is, the relation between the input and the output of a sensor, when the input does not vary significantly with time. On the other hand, dynamic characteristics describe the performance of the sensor taking account of the variation of the stimulus with time. Environmental conditions are all those factors that interfere with the sensor mechanisms and thus change its response to the input stimulus. Finally, structural related characteristics result from the specific design and components of the sensor.

Nanostructure materials exhibit great gas-sensing properties with respect to coarser grain size. This feature is determined by the large fraction of atoms confined at the surface of the constituent domains and by assuming the main interaction occurred at grain boundaries. The higher surface-to-volume ratio, inherent in SnO_2 as well as TiO_2 nanostructure offers better sensitivity for gas sensor [4]. Unfortunately, most of the existing devices also react in the presence of different gases, thus showing a low level of selectivity. To overcome this problem, the electronic-nose (e-nose) approach [34, 36] has been adopted: it uses an array of sensors having different chemical-physical characteristics and employs an intelligent device (e-nose net) to analyze the signals produced by the array and extract the desired information. The use of nanostructured materials, as applied by Laszlo [34] in his work, offers new possibilities of improving sensitivity.

3.3.1 Electrical measurements

Conductometric measurements for thin films require that proper electrical contacts are made on the layer surface. The contacts could either be permanent or permit separation and rejoining. The fabrication of stable three phase boundaries between metals, oxides and the gas phase is a common problem in gas sensor development. Usually, the electric contacts with the sensing material should be ohmic, should not diffuse into the sensing material and should not interact with the gas phase [39]. An ohmic contact may be defined as a metal-semiconductor contact that has a negligible contact resistance relative to the bulk resistance of the semiconductor. A satisfactory ohmic contact should not significantly degrade device performance, and should pass the required current with a

voltage drop that is small compared to the drop across the active region of the device [3]. Diffusion of electrode material into the sensing layer is a common source of long-term drifts. In order to prevent diffusion, a barrier layer may be deposited between the electric contact and the sensing material [9]. Electrode interaction with the gas phase may be used sometimes to improve sensor performance, but more frequently it might be a source of uncontrolled interference to the device output. The interaction mechanisms between the gas phase and the sensing material involve mainly physisorption, chemisorption, surface defects, bulk defects or three phase boundary processes [39].

3.3.2 Surface resistivity measurements

Surface resistivity is a measure of the material's surface inherent resistance to current flow. Good contacts provide a uniform contact resistance over the contact – film interface and therefore a uniform electric field over the thin film layer [39]. Unlike electrical changes that occur in the bulk of semiconducting oxides, surface conductance does not depend as heavily on the defect chemistry of the oxide but surface conductivity changes occur when a reactive gas changes the equilibrium condition of the sensor surface by combusting upon it or when the partial pressure of oxygen in the atmosphere is altered. In both of these cases, the amount of adsorbed oxygen on the metal oxide surface changes. Frequently large changes in resistance accompany these events.

This useful sensing property of metal oxides comes from the fact that in (n-type) semiconductors, oxygen lattice defects can act as electron donors. When oxygen atoms arrive from the gas phase, they remove electrons from the donors near the surface and become adsorbed as negative ions [3]. The depth of the layer is known as the Debye

length, and when the oxide crystallite size is larger than twice this dimension, the potential barrier at the grain boundary becomes a major factor in dictating the sensor resistance [21]. Because relatively small concentrations of reactive gases can cause large conductance changes in this system, a sensor with this operating mechanism depends heavily on diffusion and reactions on the sensor surface and within the porous sensor mass.

3.3.3 Four point probe (FPP)

A material's surface resistivity can be measured using either a two- or a four-point probe method. The probes can be aligned either linearly or in a square pattern contact with the surface of the material. Both two- and four-point probe methods are popular due to their abilities to minimize the parasitic effect of contact resistance. The FPP setup measures resistivity in a uniform square plane lamina with four line contacts placed on its edges as shown in *Fig 3.1*. The surface under test (SUT) is assumed to be of uniform thickness and doping level.

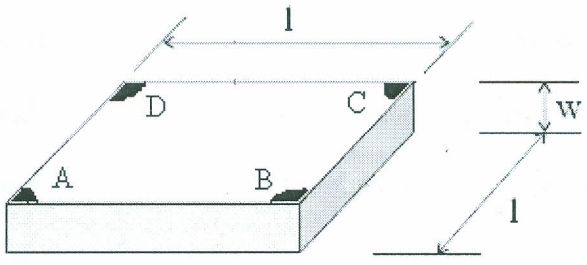

Fig 3.1: Four point probe setup.

where A, B, C and D are the four contact points at the surface of the square lamina of side l and w is the film thickness.

Practical issues in making probe tips for FPP measurements are concerned with the type of probe, probe loading and accuracy of probe spacing, means of bringing the probes into contact with the surface of the semiconductor, preparation of the semiconductor surface, magnitude and control of current. It is important that all the probes are brought into contact with the semiconductor surface with equal pressure without damage to the surfaces of the films and ensuring that ohmic contact is made with the surface.

Van der Pauw theorem [39] explains a practical method of determining the conductivity of a material given a sample in the form of a wafer of uniform thickness. When a current is injected through one pair of contacts, voltage is measured across the remaining pair of points. By Ohms law R_{ABCD} can be defined as

$$R_{ABCD} = \frac{V_{AB}}{I_{CD}} \tag{3.1}$$

Where V_{AB} is the voltage measured between contacts A and B when a current I_{CD} is driven between C and D. V_{AB} is defined positive if voltage at A is higher than voltage at B. Three other values of resistance can be obtained from the setup, these are, R_{ADCB}, R_{ACBD} and R_{BDCA}. Current driven between two adjacent sides leads to resistivity, while current between non-adjacent sides leads to Hall voltage.

For four contacts on the boundaries of a semi-infinite plane sheet, the resistances R_{ABCD} and R_{BCDA} are related by the Van der Pauw expression given by

$$\exp\left(\frac{-\pi w R_{ABCD}}{\rho}\right)+\exp\left(\frac{-\pi w R_{BCDA}}{\rho}\right)=1 \tag{3.2}$$

where w is the film thickness and ρ is the resistivity of the SUT.

Eqn. (3.2) can be simplified to

$$\rho=\frac{\pi w}{\ln 2}\left(\frac{R_{ABCD}+R_{BCDA}}{2}\right)f(Q) \tag{3.3}$$

where the correction factor f is a function of Q, which is defined as

$$Q=\frac{R_{ABCD}}{R_{BCDA}} \tag{3.4}$$

and f satisfies the relation

$$f=1-0.34657\left(\frac{Q-1}{Q+1}\right)^2-0.09236\left(\frac{Q-1}{Q+1}\right)^4 \tag{3.5}$$

It is possible to measure four resistances, R_{ABCD}, R_{BCDA}, R_{CDAB}, R_{DABC}, and evaluate ρ for each and take the mean value. ρ in Eqn. (3.3) applies to an arbitrary shape. However,

there is an advantage in using a symmetrical shape such as a disc or a square. ρ is essentially concerned with sheet resistance of a sample R_s which is defined as the resistance between opposite edges of a square of arbitrary dimensions. The sheet resistance can be as.

$$R = \int_{l_1}^{l_2} \frac{\rho\, dx}{2\pi w x} \tag{3.6}$$

from a given probe position s

$$R = \int_{s}^{2s} \frac{\rho\, dx}{2\pi w x} = \frac{\rho}{2\pi w} \ln 2 \tag{3.7}$$

for a square of side l

$$R_s = \frac{\rho l}{w l} = \frac{\rho}{w} \tag{3.8}$$

The sheet resistance in equation (3.8) is independent of l and is therefore a property of the sheet. The physical unit for R_s is Ohms (Ω), although it is also common practice to refer to R_s in terms of Ohms per square, (Ω/square).

3.3.4 X-ray fluorescence (XRF)

When a primary X-ray excitation source from an X-ray tube or a radioactive source strikes a sample, the X-ray can either be absorbed by the atom or scattered through the material. An X-ray can be absorbed by the atom transferring all of its energy to an innermost electron, during this process, if the primary X-ray has sufficient energy, electrons are ejected from the inner shells, creating vacancies which present an unstable condition for the atom as illustrated in Fig. 3.2.

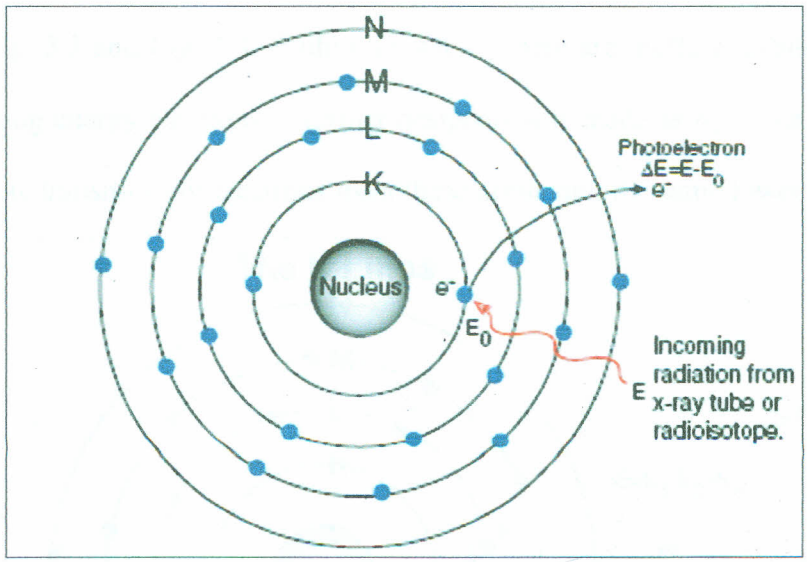

Fig. 3.2: An electron in the K shell is ejected from the atom by an external primary excitation X-ray creating a vacancy [40].

As the atom returns to its stable condition, electrons from the outer shells are dropped to the inner shells and in the process give off a characteristic X-ray whose energy is the difference between the two binding energies of the corresponding shells. The emitted X-rays produced from this process are called X-ray fluorescence (XRF). The process of detecting and analyzing the emitted X-rays is called "X-ray Fluorescence Analysis." In most cases, the innermost K and L shells are involved in XRF detection.

A typical X-ray spectrum from an irradiated sample will display multiple peaks of different intensities. The characteristic X-rays are labeled as K, L, M or N to denote the shells they originated from. Another designation alpha (α), beta (β) or gamma (γ) is made to mark the X-rays that originated from the transitions of electrons from higher shells. Hence, a K_α X-ray is produced from a transition of an electron from the L to the K shell, and a K_β X-ray is produced from a transition of an electron from the M to a K shell, as illustrated in Fig. 3.3 and Fig. 3.4. Within the shells, there are multiple orbits of higher and lower binding energy electrons, a further designation is made as α_1, α_2 or β_1, β_2, and so forth to denote transitions of electrons from these orbits into the same lower shell.

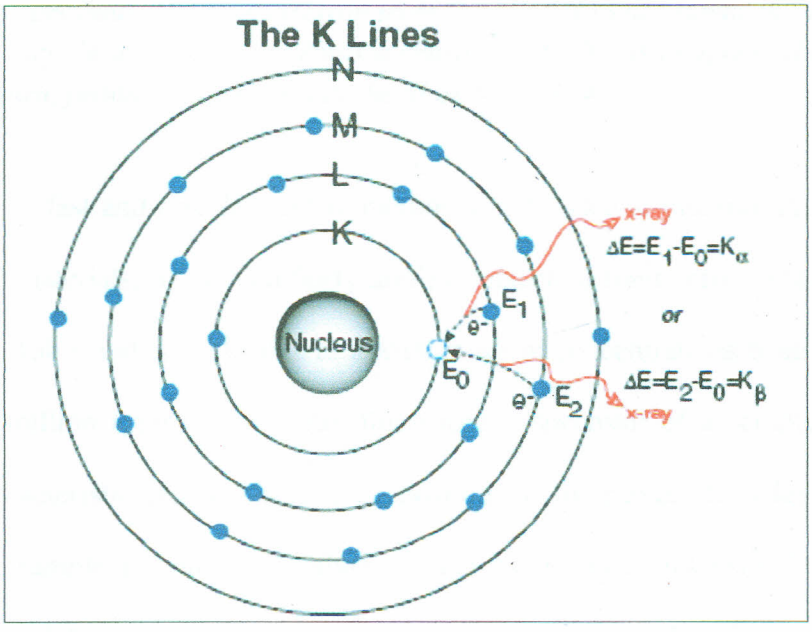

Fig. 3.3: An electron from the L or M shell "jumps in" to fill the vacancy. In the process, it emits a characteristic X-ray unique to this element and in turn, produces a vacancy in the L or M shell. [40]

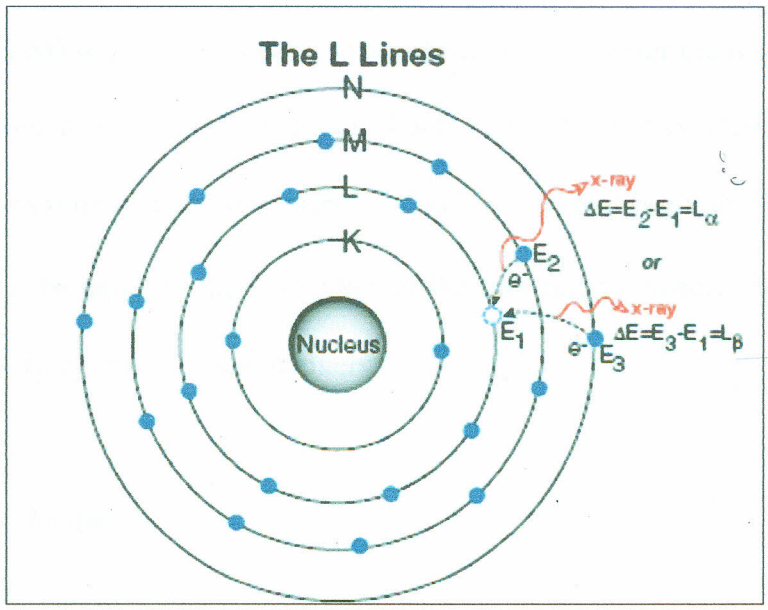

Fig.3.4: When a vacancy is created in the L shell by either the primary excitation X-ray or by the previous event, an electron from the M or N shell "jumps in" to occupy the vacancy. In this process, it emits a characteristic X-ray unique to this element and in turn, produces a vacancy in the M or N shell [40]

XRF method is a fast and non-destructive method widely used to measure the elemental composition of materials, it offers a fairly uniform detection limit across a large portion of the Periodic Table and is applicable to a wide range of concentrations from 100% to a few parts per million (ppm). The X-ray fluorescence spectrum of a sample reveals a number of characteristic peaks. The energy position of the peaks identifies the atoms present in the sample (qualitative analysis), whereas the peak intensity leads to the relative or absolute elemental composition of the sample (semi-quantitative or quantitative analysis). The XRF analysis has a broad spectrum of applications in diverse fields, including, determination of heavy metals in soils, sediments, waters and aerosols, on geology for quantitative and qualitative analysis of clays, minerals and rocks [40].

3.3.5 Thin film optics

Electromagnetic (EM) waves propagating in a material usually enter the material through a boundary between it and another medium. Each incident wave is accompanied by a reflected and a transmitted wave. The intensity I_o of the incident beam to the surface of a solid medium must be equal to the intensities of the transmitted, absorbed and reflected beams denoted by I_T, I_A and I_R. Alternatively

$$T+R+A=1 \tag{3.9}$$

where T, A and R represent, respectively, transmissivity $\left(\frac{I_T}{I_o}\right)$, absorptivity $\left(\frac{I_A}{I_o}\right)$ and reflectivity $\left(\frac{I_R}{I_o}\right)$. Consider light normally incident on a material with a smooth polished surface of refractive index n_1 as shown in *Fig. 3.5*

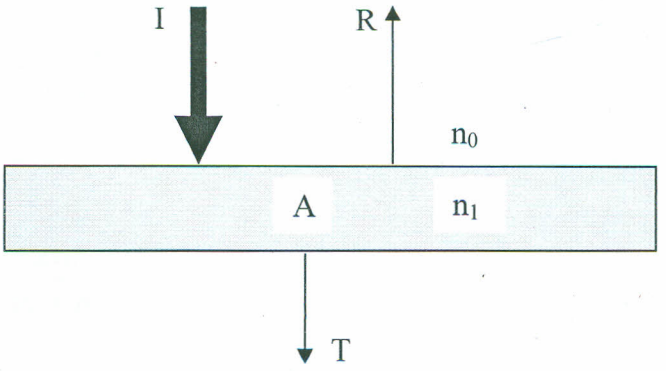

Fig. 3.5: Reflection and transmission of a two-material medium interface

The optical constants, refractive index (n) and the extinction coefficient (k) describe how light propagates through the film; n is a measure of how much the speed of the incident EM wave is reduced inside the material and represents propagation without absorption, while k represents an exponential damping due to absorption within the material. For the two-material medium interface, the Fresnel coefficients for the amplitudes of the reflected and transmitted light travelling from n_o (the surrounding medium) to n_1 are given in equations (3.10) and (3.11) [15, 41].

$$r = \frac{n_o - n_1}{n_o + n_1} \tag{3.10}$$

$$t = \frac{2n_0}{n_0 + n_1} \tag{3.11}$$

For light travelling from n_1 to n_o the reflected and transmitted amplitudes are given by eqns. (3.12) and (3.13).

$$r' = \frac{n_1 - n_0}{n_1 + n_0} \tag{3.12}$$

$$t' = \frac{2n_1}{n_1 + n_0} \tag{3.13}$$

R and T can be expressed as a products of the amplitudes' coefficients $r.r'$ and $t.t'$. For absorbing films with an absorption coefficient k_1, the refractive index takes a complex form $n_1 - ik_1$, hence the reflectivity

$$R = \frac{(n_0 - n_1)^2 + k_1^2}{(n_0 + n_1)^2 + k_1^2} \tag{3.14}$$

If a thin film is deposited over the surface of the material there are now 2 interfaces where the light can be reflected and transmitted as shown in Fig. 3.6. Also, there will essentially be an infinite number of multiple reflection and transmissions that need to be summed to give the final amount of reflected and transmitted light. This sum is related to the optical properties of the film, the optical properties of the substrate, their relative values and the phase thickness of the film, that is, n_o, n_1, n_2, w *and* λ [41].

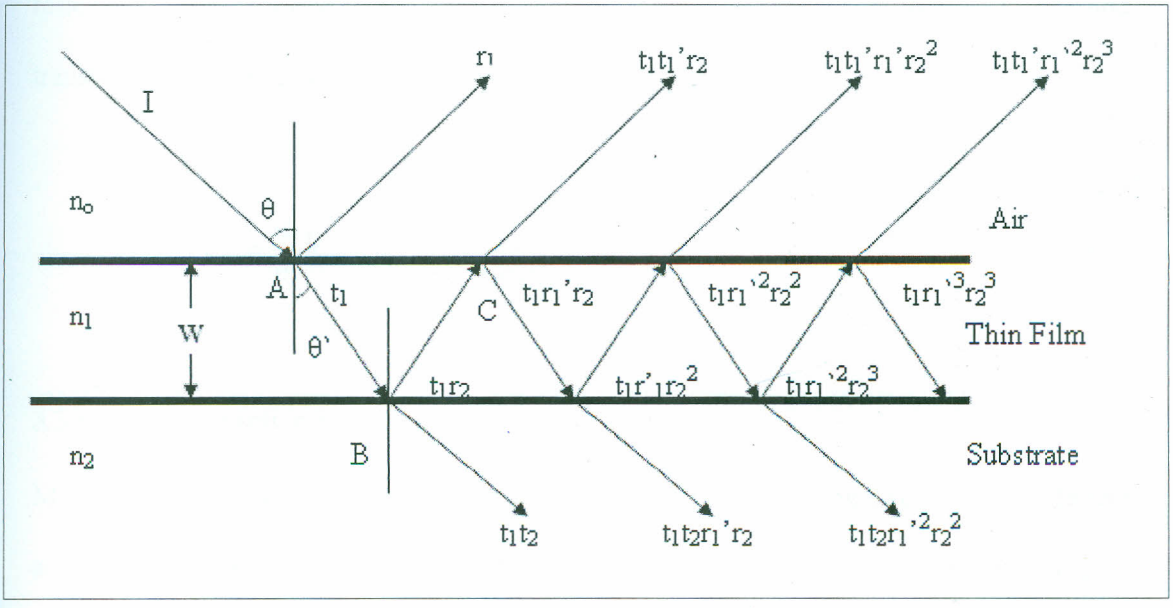

Fig. 3.6: Transmission and reflection on a thin film single layer coating

Each of the interfaces A and B in Fig. 3.6 offer reflection and transmission whose amplitudes are given by equations (3.10 - 3.13), with a modification of the Fresnel coefficient on the film-substrate interface where the subscripts 0 and 1 are changed to 1 and 2 to make the results applicable for the film (n_1) – substrate (n_2) interface. Summing

the multiply transmitted beams whose amplitudes decline with repeated interfacial impingement results in an infinite geometric series that has a common ratio $r_1' r_2 e^{-2i\delta}$ and has a finite sum because $r^2 < 1$. Taking $r' = -r$ results in

$$t = \frac{t_1 t_2 \, e^{-2i\delta}}{1 + r_1 r_2 \, e^{-2i\delta}} \tag{3.15}$$

In the experimental setting, the quantities of interest are the ratios of the intensities of the transmitted and reflected waves to that of the incident wave. The intensity of an EM wave is proportional to the square of its amplitude [42]. The ratios of the intensities of the reflected and transmitted waves to that of the incident wave are called the reflectance and transmittance, respectively. The transmittance (T) is given by

$$T = \frac{n_2}{n_1} |t_{12}|^2 = \frac{n_2}{n_1} \frac{4n_1^{\,2}}{(n_1 + n_2)^2} \tag{3.16}$$

3.3.6 The refractive index (n)

Materials are characterised optically by their optical constants, the extinction coefficient and refractive index. The extinction coefficient k is the imaginary part of the complex refractive index, assumes the role of an index of attenuation. The refractive index n is a measure of how much the speed of the incident EM wave is reduced inside the material and represents propagation without absorption. The transmittance spectrum is used to calculate the refractive index from equation (3.16). The refractive index obtained is

wavelength dependent, that is $n(\lambda)$, and the value obtained is stated with reference to a specified wavelength of the EM spectrum.

3.3.7 Film porosity

The porosity is a function of the film refractive index [18] and is calculated as

$$Porosity = \left(1 - \frac{n^2 - 1}{n_d{}^2 - 1}\right) \times 100 \qquad (3.17)$$

Where n_d is the refractive index of pore-free anatase ($n_d = 2.40$) and n is the refractive index of the porous thin film

3.4 TiO_2 Thin Films

TiO_2 has a density of 4230 Kg/m^3, a bulk density of 850 Kg/m^3, melting point of 1870°C and a boiling point of 2972°C, two tetragonal phases, anatase and rutile as illustrated in Fig 3.7a and 3.7b,

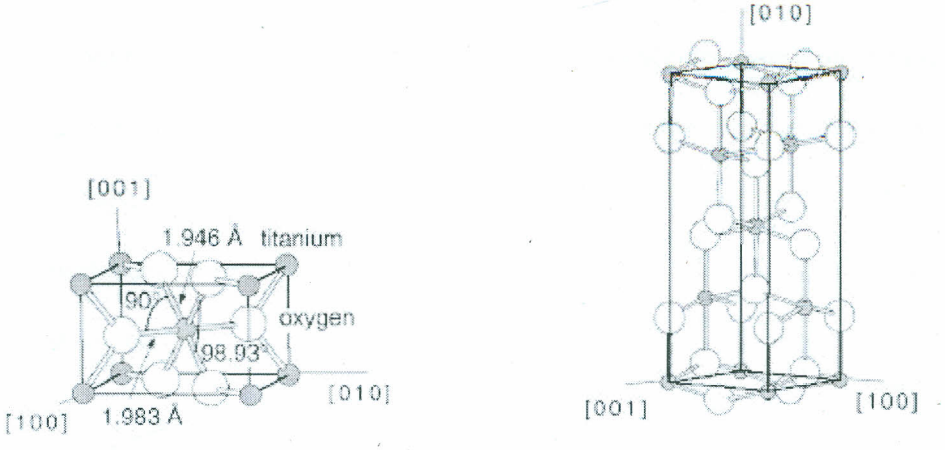

(a) Rutile *(b) Anatase*

Fig 3.7: Unit cell parameter for TiO_2 crystalline phases of [3]

The starting form of a material can influence its final properties as a film layer as well as its ease of evaporation and titanium dioxide is a case in point. Many oxidation states exist for titanium oxide, some requiring very high evaporation temperatures, and some requiring high background oxygen pressures to fully oxidize, which in itself leads to film density problems. Many studies with different compositions have been carried out by researchers seeking the best starting material composition [38]. It is generally agreed that Ti_3O_5 is the easiest and most successful composition to start with because it melts, whereas the other compositions either do not melt or dissociate to the degree that low absorption films cannot be grown. Some compounds sublime or form fused surfaces, both leading to spatter and excessive outgassing and high absorption. Since Ti_3O_5 melts, there is no possibility of trapping moisture that can produce outgassing and spitting.

Titanium (Ti) and oxygen form a number of stable phases, the most practical being TiO, TiO_2, Ti_2O_3 and Ti_3O_5, any of which can be evaporated and subsequently oxidized to the final stable phase TiO_2. Whenever any of the various oxide states of titanium is evaporated, the vapour consists of various Ti-O combinations which change in oxygen content as the evaporation proceeds. The refractive index of the deposited film is thus not constant because most Ti-O_x materials evaporate incongruently. Starting with Ti_3O_5 composition ensures that the only titanium species in the vapour is TiO and the oxygen content in the vapour remains constant [35].

When heated above its melting point, TiO_2, decomposes into suboxides and liberate oxygen. It is therefore necessary to prepare a dense homogeneous slug of melted material

by melting at low power before beginning evaporation [38]. To promote complete oxidation and correct stoichiometry of the oxide compound, metal oxides require a partial pressure of oxygen and deposition rate of 2 to 5 Å/s at substrate temperatures of 200°C to 250°C. This is important in producing the desired physical properties such as refractive index, transparency and mechanical durability of the film layer. As TiO_2 crystallizes, the nature of the film formed is influenced by the density of the adatoms arriving on the wafer as evidenced by the formation of anatase and rutile phases [41]. The method of film preparation and the conditions in each methodology directly affects the optical constants of the film.

3.5 Sensitivity of TiO_2 to LPG

Optimization of sensor performances requires a systematic characterization of the materials' properties, a good knowledge of the dependence of those properties on the preparation processes and a proper understanding of the sensing mechanisms. Usually, a single characterization technique produces useful data to the study of more than one of the referred aspects, so that the advances observed in one field also bring significant advances to the others.

Thin film gas sensitivity is observed to increase when crystalline diameter is comparable to the Debye length of the semiconductor [21]. The response of TiO_2 sensor to LPG is expressed in terms of the relative variation ΔR of the sensor resistance to a given concentration of the vapour. In most publications ΔR, is used to represent sensitivity [11, 21].

$$\Delta R = \frac{R_o - R_g}{R_o} x\, 100\% \qquad (3.18)$$

Where R_g is the resistance of the film when exposed to an atmosphere containing a known concentration of the LPG and R_o is the resistance of the film when exposed to air.

CHAPTER FOUR

MATERIALS AND METHODOLOGY

4.0 Introduction

In this chapter, the equipment and materials used in the study are introduced and discussed in terms of their functions, limits and dimensions in relation to the study. The set-ups and the experimental procedures have also been described as they link the equipment to the theoretical background.

4.1 Substrate Cleaning

Microscope glass slides (75 x 25 x 1 mm^3) were used as substrates in this work. The substrates were cleaned by soaking in saturated sodium hydroxide solution for 15 minutes; this slightly etched the glass surface which ensured the removal of surface residues, followed by a 5 minutes dip in 1molar hydrochloric acid to neutralize the alkaline etching effect on the glass surface and finally the glass slides were rinsed in de-ionized water for 20 minutes [44]. The wet glass was dried by blowing air over the surface and then wiped using cotton swabs. The slides were placed into the deposition chamber after cleaning to minimize surface contamination in air. Protective hand gloves were used to handle the slides after cleaning to avoid contaminating the surfaces.

4.2 Deposition Process

TiO_2 thin film was coated onto microscope glass slides using Edwards Auto 306 system (Fig 4.1) installed in the Department of Physics at Maseno University. Besides thermal evaporation used in this study, the system can also be used for sputtering (both RF and

DC). Thermal evaporation was the preferred deposition method in this study due to its advantage of deposition in small scale, high deposition rate and the nature of the source material being in pellet form.

Fig 4.1: Edwards Auto 306 coating unit.

A crystal monitor installed in the system with a quartz vibrator was used to monitor evaporation rates as discussed in section (2.2.4). High vacuum in the chamber was maintained by RV8 rotary pump backed by EXT 501 turbo-molecular pump. The system was cooled by running water whose temperature was lowered by dipping ice-blocks in the water to prevent overheating of the pumps. The source material, TiO_2 in pellet form, was supplied by BOC Edwards Company and had a purity of 99.9% at packing. The glass slides in packs of 100 were obtained from local laboratory equipment stores.

The coating system was operated for TE as per the instruction of the manual [45]. TiO_2 in pellets were ground to fine powder using a pestle and mortar and placed into a molybdenum boat inside the vacuum chamber for melting. Using scotch tape, the glass

slides were mounted on the rotary substrate holder as shown in Fig. 4.2, two extreme ends of the slides were masked off to produce a step for film thickness measurements.

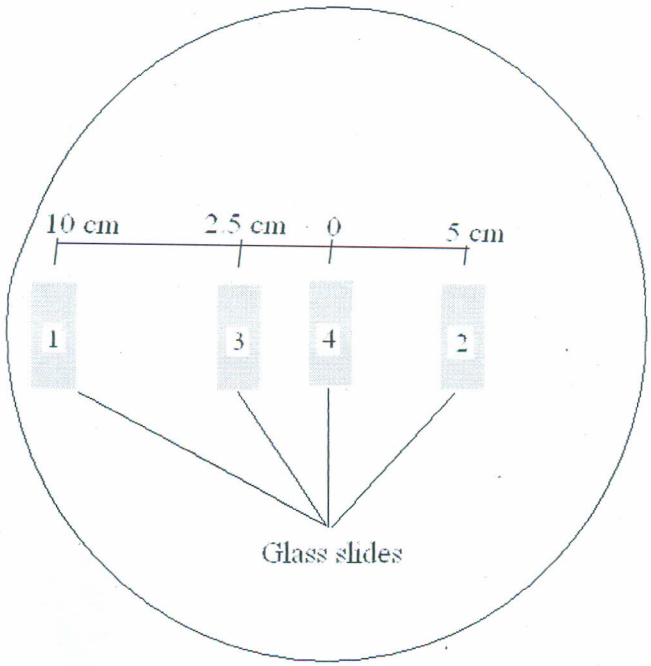

Fig. 4.2: Glass slide mounted on substrate holder

glass slide are numbered with 1 being furthest from the centre of the substrate holder at 10 cm and 4 being at the centre of the holder.

The substrate-boat distance was maintained at 20 cm for all the samples. After closing the chamber, the system was evacuated to a base pressure of about 10^{-5} mbar following the manual instructions [45]. The manual shutter arm was kept in a closed position, then the evaporator control was turned to low tension (LT) mode and the heating primary current steadily raised for the titanium dioxide in the boat to melt to a red metallic slug, this was monitored through the observing window. The substrates were rotated through the deposition process to improve on the film thickness uniformity. When the molten slug

was ready to vaporize, the shutter was opened and different samples were prepared by varying the chamber pressure, deposition time, substrate location and the heating current in an attempt to optimize the deposition conditions. These variables directly influenced the film's physical and optical characteristics.

4.3 XRF Analysis

XRF measurements were done at the Ministry of Environment and Natural Resources, Mines and Geology Department using a Philips minipal 2 XRF machine whose schematic diagram is shown in Fig. 4.3. The machine was interfaced with a computer using minipal/mate software.

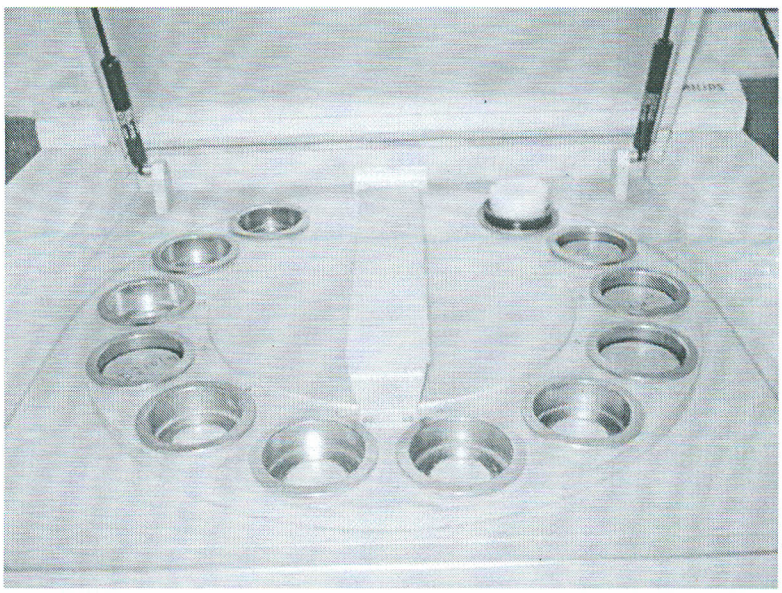

Fig. 4.3: Philips minipal 2 XRF machine

The coated glass slides were mounted on top of the holes, hence several samples could be analyzed at the same time.

4.4 Optical Analysis

The optical analysis was done using Spectro 320 optical spectrum analyser (SP320) unit shown in Fig. 4.4.

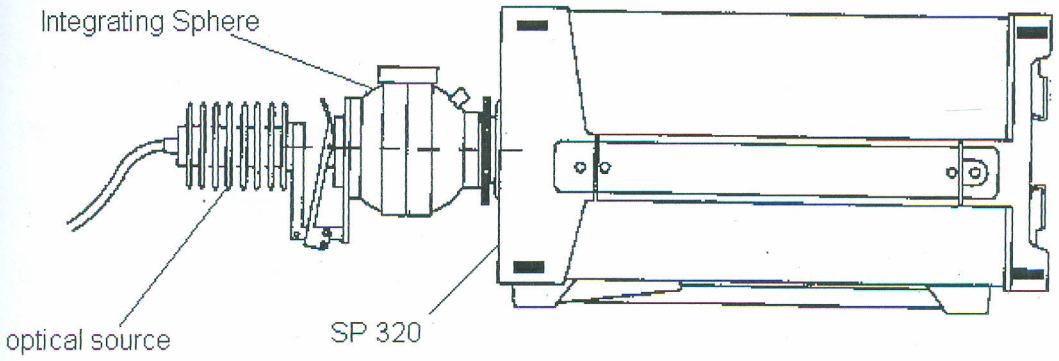

Fig. 4.4: Spectro 320 optical spectrum analyser (side view) [SP 320]

The unit was interfaced with a computer using IS Specwin (version 1.5) software which was used to plot the measured spectrum from the specimen. The coated slide was mounted onto the integrating sphere provided with the SP320 unit. A 45° beam trap was inserted into the sphere to reduce direct lamination. The detectors chosen for this study were photomultiplier (PMT 1) with a spectral range of 190 nm to 850 nm and indium gallium arsenide (InGaAs) whose spectral range is 800 nm to 1700 nm. The two detectors' overlap allowed for a continous spectral measument of 190 nm to 1700 nm.

The TiO_2 thi n films transmittance and reflectance spectrum were measured using a SP320. The samples were mounted on an integrating sphere connected directly to the equipment at the optical port and illuminated by 10 V 0.8 A lamp. The spectral range measured for this study was 300 nm to 1700nm. The spectrum was compared to another set measured using DUV spectrometer found at the Department of Physics, University of

Nairobi. The results showed slight variation which could have been due to the positioning of the samples. Hence, the results from the SP320 were used throughout.

4.5 Film Thickness Measurements

Measurement of the film thickness was done at University of Nairobi, Department of Physics laboratory using Alpha-step IQ surface profilometer (Alpha-step IQ) interfaced with a computer Fig. 4.5. Alpha-step IQ is a sensitive profilometer with 0.1% precision that measures roughness, waviness and step height of surface coatings.

Fig. 4.5: Alpha-step IQ surface profilometer

The computer interface with the profilometer was used to control the operations and displays the results. The profilometer characterized surfaces by scanning it with a

diamond tipped stylus while the stylus rested on the sample surface, a transductive sensor registered the vertical motion of the stylus.

The TiO_2 films were prepared with two steps to the substrate by masking-off parts of the glass slide with a tape forming a square before deposition to allow for thickness measurement by a surface profiler [15]. The measurements were done using Alpha-step IQ. The scan was run from right to left taking peak measurements with a stylus force calibrated at 18.5 mg and a scan length of 1500 μm. To measure a step height, the scan traces across the step region from the uncoated substrate up to the coated film and the difference between the two values given as the film thickness, which is equal to the step height.

4.6 Electrical Characterization

Sheet resistivity measurements were done using Keithley 2400 sourcemeter (KE 2400) shown in Fig. 4.6.

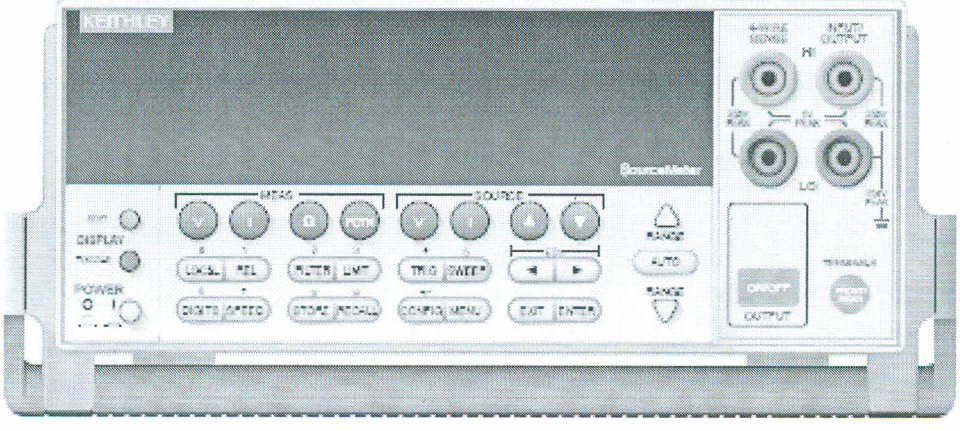

Fig. 4.6: Keithley 2400 sourcemeter front panel [43]

KE 2400 offers sourcing options for current and voltage at any specified time and can be used as a voltmeter, a current meter and an ohmmeter without changing connections [43]. This offers convenience and minimizes compatibility and synchronization errors which occur when multiple instruments are used. The sweep solution provided with the meter was used to obtain $^{I}/_{V}$ and $^{V}/_{R}$ characteristics for all the samples. The four-wire remote sensing option was employed along with the FPP method for measuring resistivity; this optimized the accuracy of measurement as opposed to the two-wire local sense-connection that is preferred for *I* sourcing and *I* measurements. Clamping action that is provided for in selecting Compliance (real or range) was used to set the sourced current value at 1.0 nA and the voltage compliance limit at 21.0 V. The instrument for measuring sheet resistance used in this work is located at Kenyatta University, Physics laboratory.

Using four point probe method, four contact points were connected to the sourcemeter and used to measure the sheet resistivity, using silver paint to enhance ohmic contact in the copper-TiO_2 contact as shown in Fig. 4.7. The contact spacing was maintained in a square shape of side 2.5 cm, taking advantage of the width of the glass slide. The other ends of the wires come out of the tube and were attached to KE 2400. Direct current (dc) was passed through the films (sourced current) and the p.d. (V) across the adjacent sides measured using KE 2400 for film with different thicknesses.

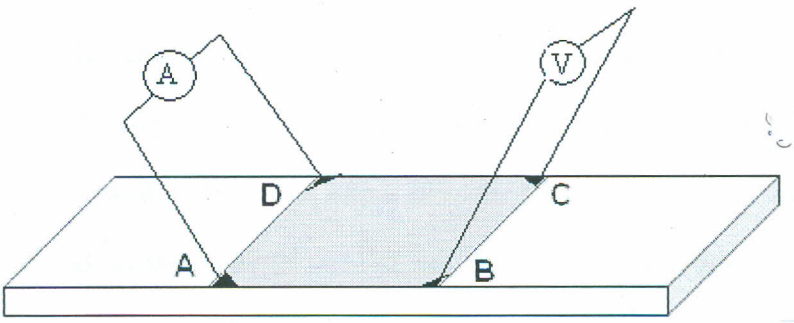

Fig. 4.7: Four point probe contact using silver paint

The setup for measuring sheet resistivity in air and LPG rich environment is shown in Fig. 4.8.

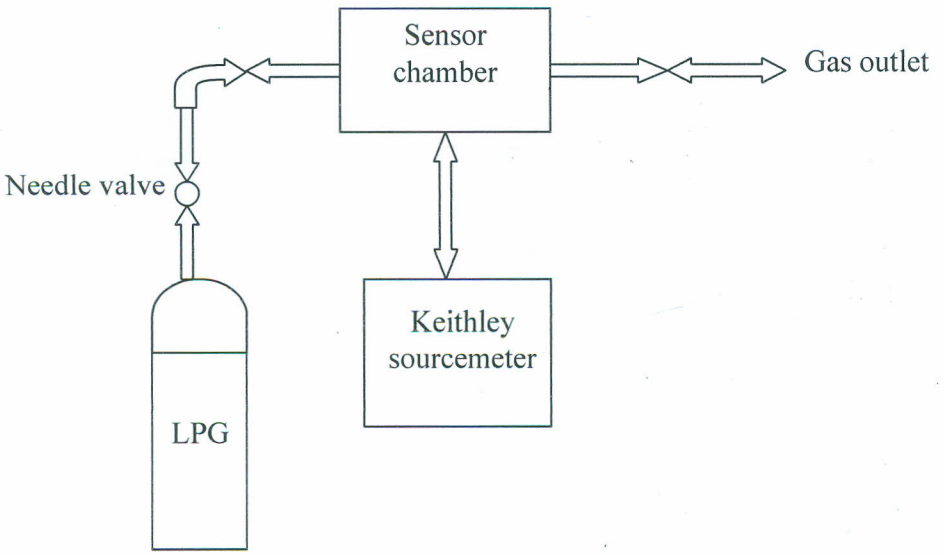

Figure 4.8: Gas sensing set-up

In this configuration, the gas was supplied from the cylinder and its flow rate was restricted by nozzles attached to the cylinders. The gas was directed through a special blown tube (from the Department of Chemistry, Kenyatta University) that allowed for the passage of wires as well as free flow of gas over the film surface. The sheet resistivity was then measured on the films in three stages; before exposure, during exposure and after exposure to LPG at 5 minutes interval with three measurements at each stage.

CHAPTER FIVE

RESULTS AND DISCUSSIONS

5.0 Introduction

The results of the study are presented and discussed in this chapter. The TiO_2 samples were prepared by thermal deposition on microscope slides. The deposited films had a square pattern to allow for measurement of resistivity by Van der Pauw setup. The characterization included XRF analysis, the optical transmittance, film thickness and sheet resistivity. Film properties such as refractive index and film sensitivity were derived from the measurements and discussed. The results obtained were compared to the others obtained in relevant studies.

5.1 XRF Analysis

Two sets of samples were obtained from the deposition process, set A were deposited at a base pressure of 1.0×10^{-4} mbar while set B were prepared at a base pressure of 6.0×10^{-5} mbar. Each of the set had four samples differentiated by the film thickness, the thickness variation was created by the positions of the substrates on the substrate holder as shown in Fig. 4.2. The substrates placed nearest to the centre of the chamber (sample 4) had thicker layers of TiO_2 film deposited, while the ones farthest from the centre (sample 1) had thinner layers.

Two samples were selected from sets A and B to ascertain the composition of the films using XRF analysis. The results are plotted in Figs. 5.1a – 5.1d

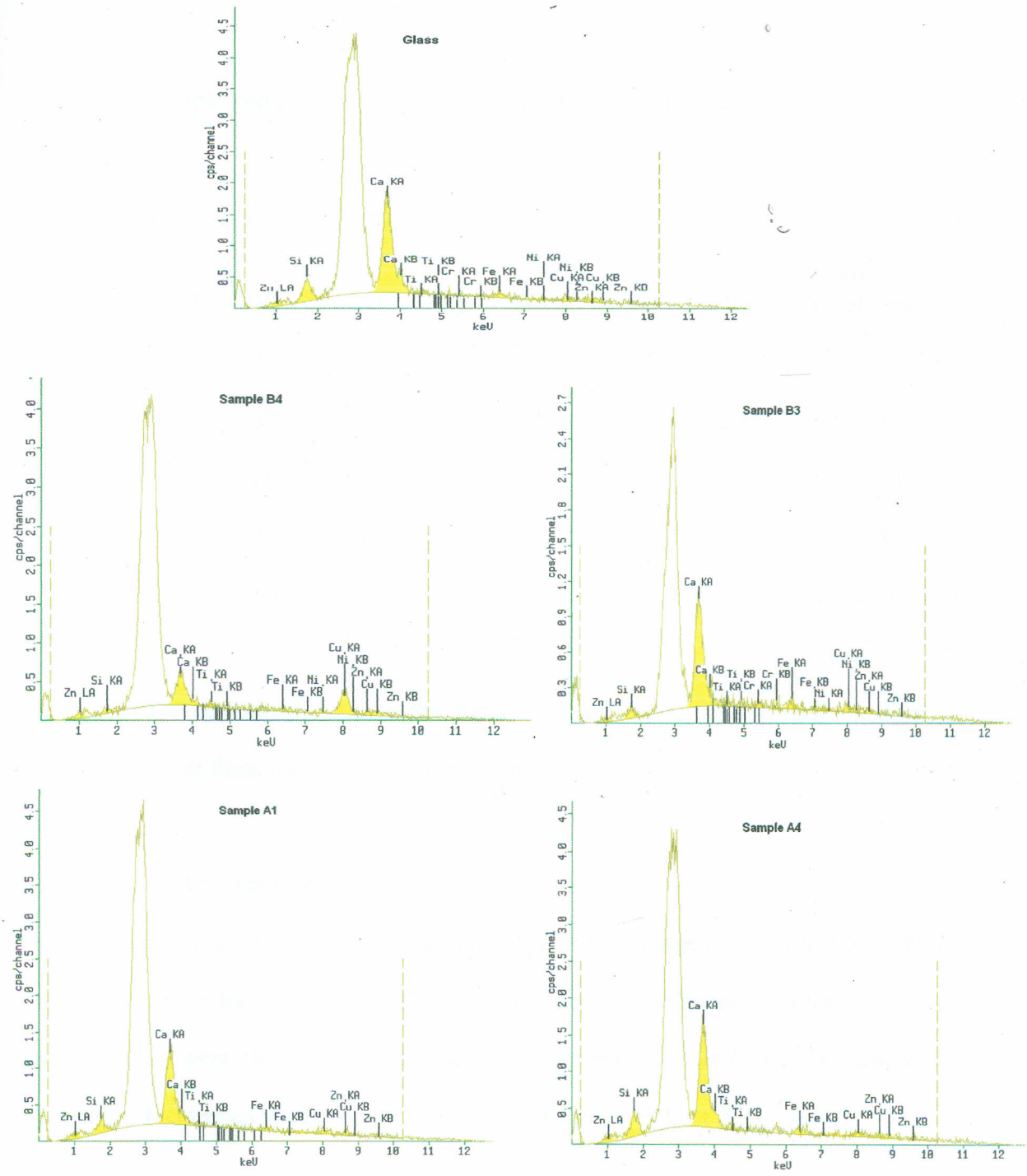

Fig: 5.1: XRF spectra for glass, B4 and B3 samples prepared at chamber pressure of 6.0×10^{-6} mbar, A1 and A4 samples prepared at a chamber pressure of 1.0×10^{-4} mbar

A tabulated sample composition from the spectra of Figs. 5.1a – 5.1d is presented in Table 5.1

Table 5.1: XRF analysis of film compositions

Compound (%) / Sample	SiO_2	CaO	ZnO	Fe_2O_3	CuO	TiO_2	Film Thickness (m)
Glass	59	37	1	1	1	0.6	
A1	57	38	1	1	2	0.8	3.28×10^{-8}
A4	59	36	0.9	1	1	1	4.58×10^{-8}
B3	57	36	1	2	2	2	1.8×10^{-7}
B4	59	32	1	1	2	3	2.3×10^{-7}

The percentage content of TiO_2 in the films is observed to increase with the film thickness. Thicker films had a higher composition of TiO_2.

5.2 Optical Transmittance

The transmittance spectra were measured in the UV-VIS-IR range (300 nm to 1900 nm) to determine the refractive index of the samples formed for different thicknesses. Two sets of samples were obtained for two different base pressures. In each set, four samples with varied thicknesses were prepared. The spectra are given in Figs. 5.2a and 5.2b.

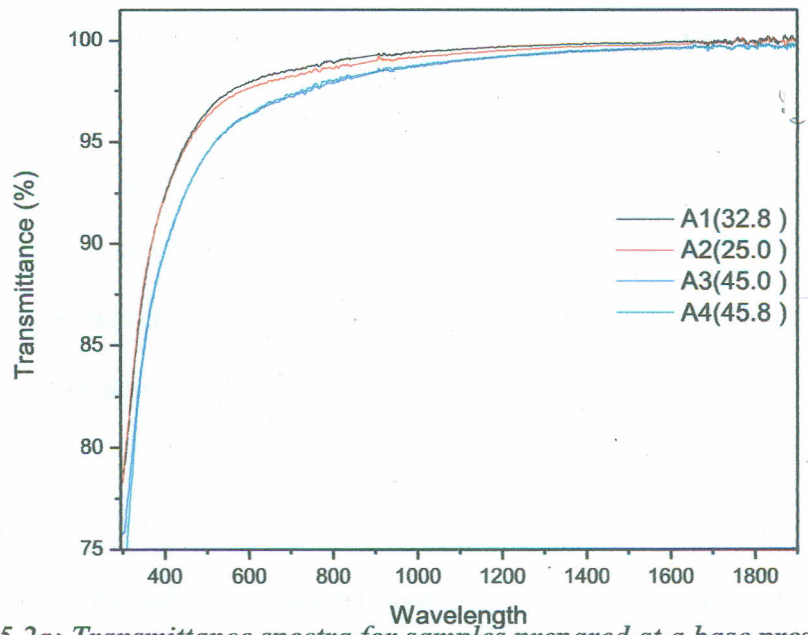

Fig 5.2a: Transmittance spectra for samples prepared at a base pressure of 1.0×10^{-4} mbar

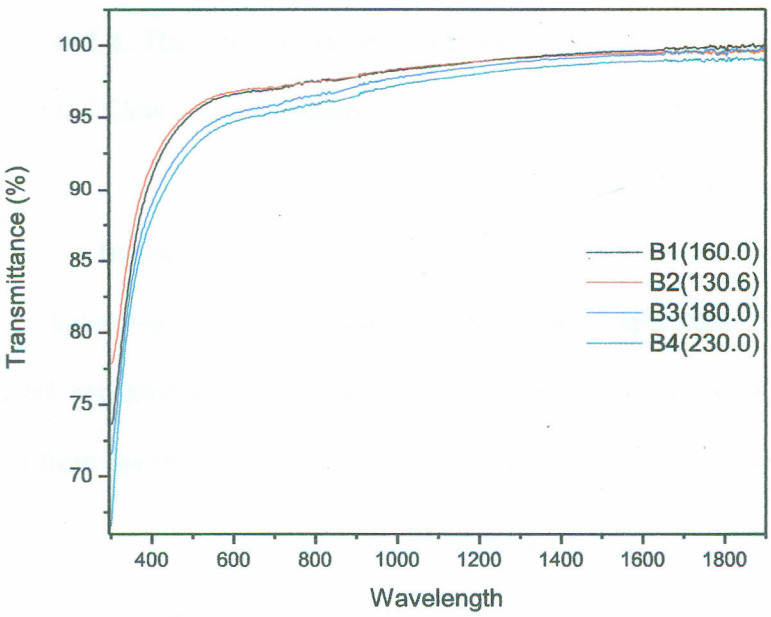

Fig 5.2b: Transmittance spectra for samples prepared at a base pressure of 6.0×10^{-5} mbar

The decrease in the transparency of the films in the UV region (below 360 nm) could be attributed to fundamental light absorption in the film or to laser damage by high energy radiation associated with shorter ultraviolet absorption edges. The change on the deposition chamber pressure had little effect on the transmittance as both samples as indicated in Figs. 5.2a and 5.2b had the highest transmittance of 96.5% and the lowest of 94.5% at 550 nm wavelength (average of 360 nm – 750 nm, the VIS range). Variation in transmittance with deposition pressure has been studied by Rao [38] and obtained similar results.

The difference in the individual spectral lines identified as A1 – A4 and B1 – B4 shown in Figs. 5.2a and 5.2b are due to variation in the sample thickness. Thinner films identified as 1 and 2 in both A and B sets showed higher transmittance than thicker films identified as 3 and 4. The reduced transmittance can be attributed to improved packing density making the films optically denser.

5.3 Refractive Index.

The refractive index was calculated from the transmittance spectrum of 4 samples A1, A4, B3 and B4 and plotted against the wavelength as shown in Fig. 5.3. The samples were selected from the original eight to represent the two deposition chamber conditions studied.

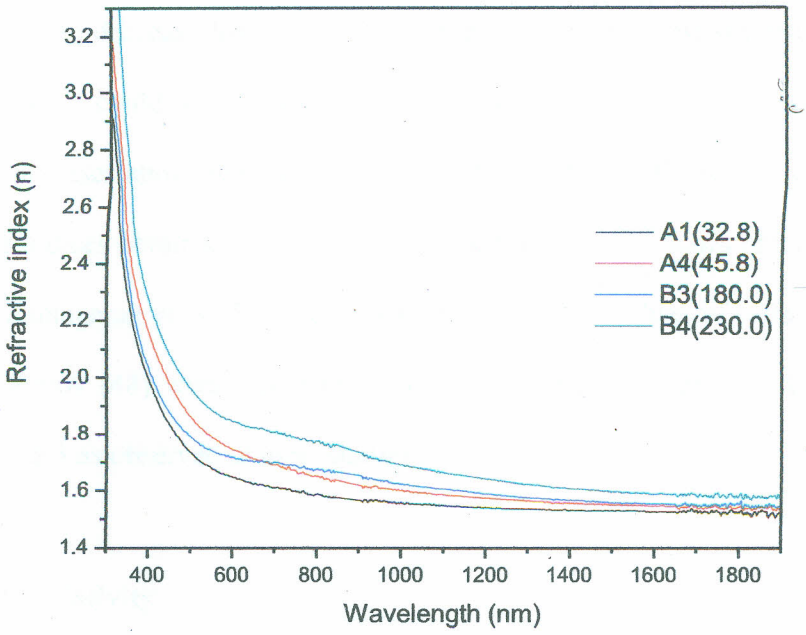

Fig. 5.3: Refractive index of TiO_2 *samples. A1 and A4 prepared at a chamber pressure of 1.0 x* 10^{-4} *mbar, B3 and B4 at a chamber pressure of 6.0 x* 10^{-6} *mbar*

The refractive indices were 1.66, 1.74, 1.79 and 1.88 for A1, B3, A4 and B4 respectively at 550 nm wavelengths. This result shows that thicker films had higher refractive indices than thinner ones in each of the base pressures selected, although B3 and B4 exhibited higher ranges of refractive indices that A1 and A4. Comparable values have been obtained by other deposition methods like dc magnetron sputtering [24, 25], RF magnetron sputtering [22, 23], sol-gel method [18] and reactive electron beam evaporation [38]. Higher indices can be attributed to packing densities which improved with increase in film thickness and decrease in deposition base pressure, as there is less gas incorporated in the film.

At short wavelength (below 400 nm), there is a high refractive index in all the films with values observed to decrease from 1.9 to 1.6 in the VIS region of the spectrum. The high refractive indices could be attributed to high dispersion which is lowered as the wavelength increases above 600 nm, leading to less variation in the index. The values of the refractive indices obtained in this study are comparable with values obtained in other studies by Karunagaran *et al* [24] and Popov [48]. The low values of refractive indices obtained by Popov [48] were raised by annealing at varied temperatures to get values comparable to 2.3 as observed in most studies [18, 22, 23, 38].

5.4 Sheet Resistivity

All the eight samples prepared under the two base pressures were treated to sheet resistivity measurements as described in section 4.6. The results were recorded from the Keithley sourcemeter and are presented in Fig. 5.4a for four samples with different film thicknesses at a deposition pressure of 1.0×10^{-4} mbar. A similar trend of results as presented in Fig. 5.4b was obtained for samples deposited at a lower pressure of 6.0×10^{-5} mbar.

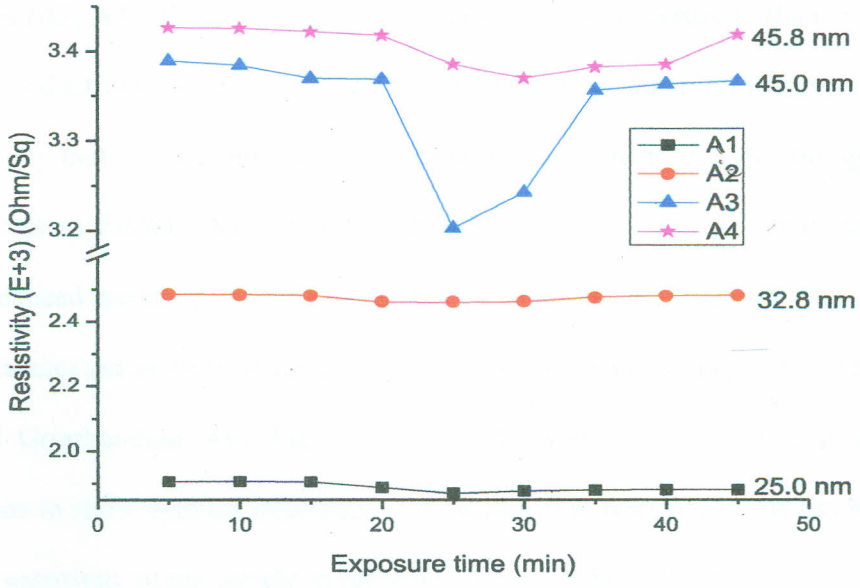

Fig. 5.4a: The sheet resistivity of TiO_2 thin films deposited at 1.0 x 10^{-4}mbar. A1, A2, A3 and A4 with different film thicknesses

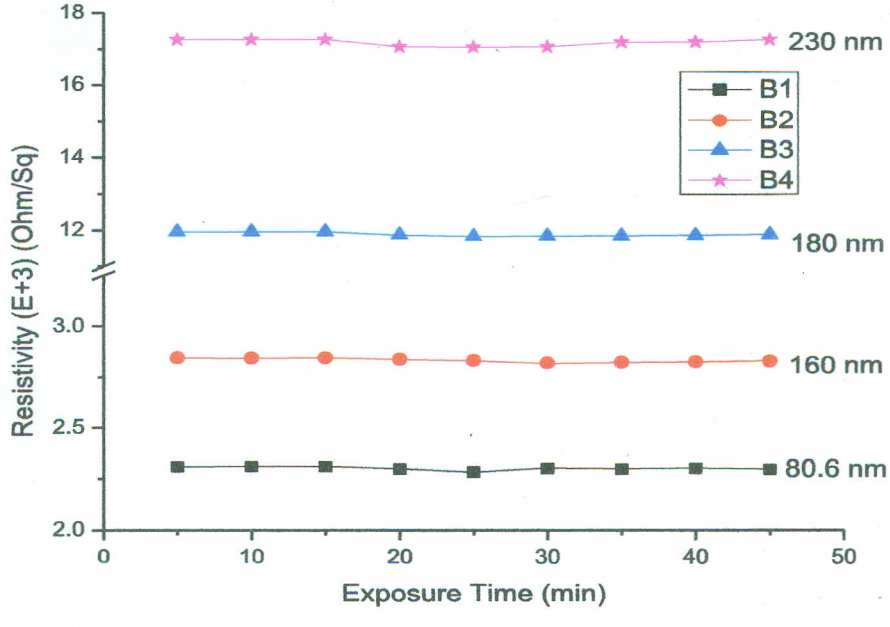

Fig. 5.4b: The sheet resistivity of TiO_2 thin films deposited at 6.0 x 10^{-5}mbar. B1, B2, B3 and B4 with different film thicknesses.

Thicker samples (A3, A4, B3 and B4) exhibited higher ranges of resistivity than thinner films. Higher conductivity can be attributed to low density in the films (from higher chamber pressure) that can be attributed to stoichiometric defects created during the deposition process as titanium has stable oxidation states of Ti^{3+} and Ti^{4+} that lead to formation of reduced oxides containing many O_2 vacancies in the material with Ti-O bonds. The vacancies act as electron donors and high leakage paths as has been observed by Sankar and Gopchandran [49]. Figs. 5.4a and 5.4b were further used to produce individual graphs to show detailed information of the thin film response to the gas being sensed, that is, sensitivity of the sample as presented in Figs. 5.5a and 5.5b.

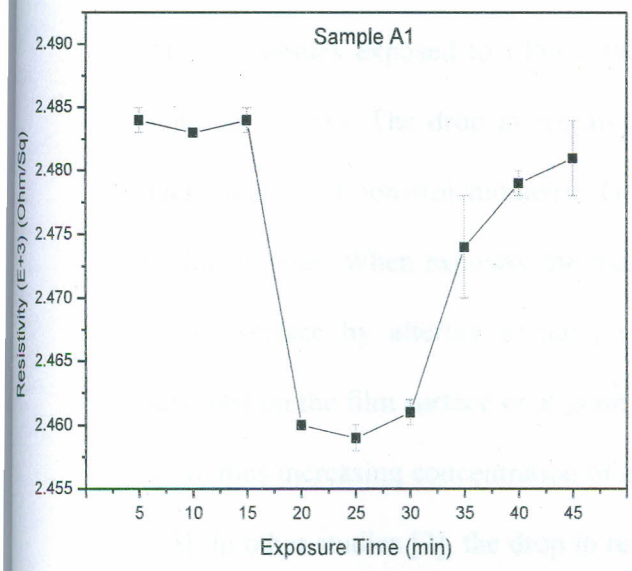

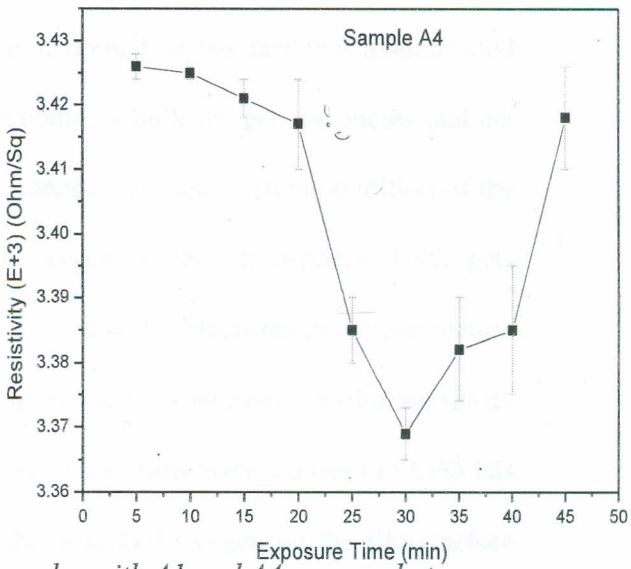

Fig. 5.5a: The resistivity of TiO_2 thin films for samples with A1 and A4 prepared at a chamber pressure of 1.0 x 10^{-4} mbar but different film thicknesses

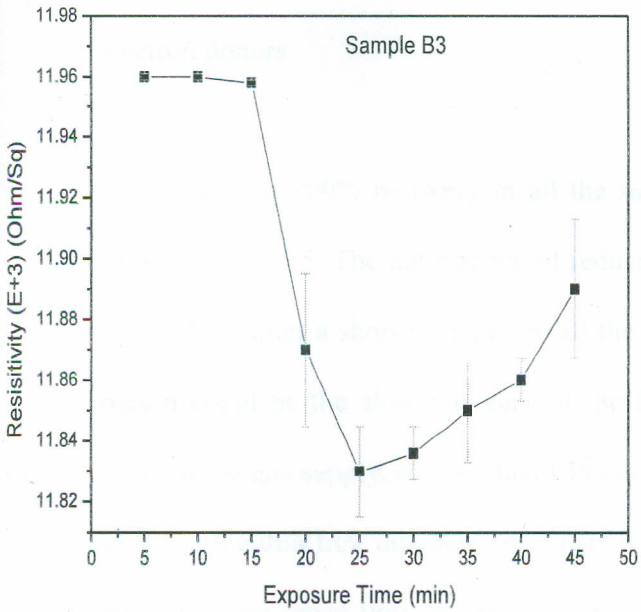

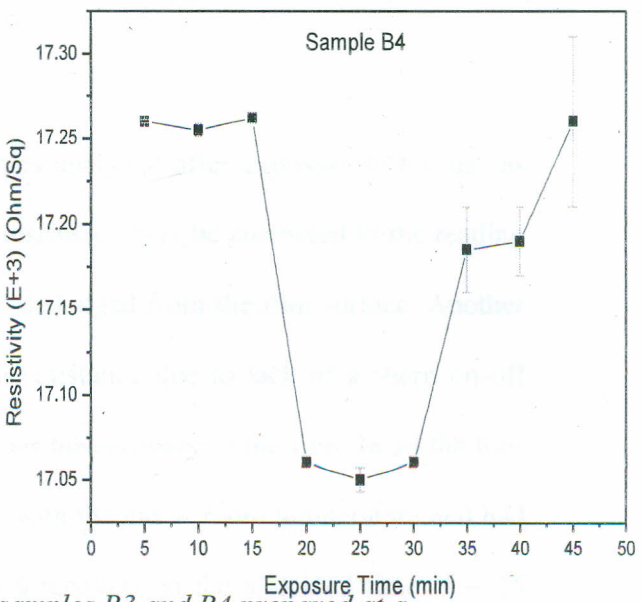

Fig. 5.5b: The resistivity of TiO_2 thin films for samples B3 and B4 prepared at a pressure of 6.0 x 10^{-5} mbar but different thicknesses.

All the samples exposed to LPG exhibited a drop in sheet resistivity when they were exposed to LPG. The drop in resistivity can be attributed to the fact that as-deposited TiO_2 consists of non-stoichiometric TiO_2 which contains bulk oxygen vacancies that act as donor states. When exposed, the reactive gas changes the equilibrium condition of the sensor surface by altering partial pressure of oxygen in the atmosphere. LPG gets adsorbed on the film surface or at grain boundaries; it donates electrons to the conduction band, thus increasing concentration of electrons allowing for a decrease in film resistivity [13]. In other studies [2], the drop in resistance when the films were exposed to LPG has been attributed to the reaction of the gas with the adsorbed oxygen on the film surface and at the grain boundaries and hence increased conductivity. The results shown in Fig. 5.5 are consistent with results obtained for response of TiO_2 to reducing gases like CO [2, 3], which shows that TiO_2 is an n-type semiconductor, that is, O_2 lattice defects act as electron donors

There was no 100% recovery in all the samples analyzed after exposure to the gas as shown in Fig. 5.5. The appearance of reduced resistance may be attributed to the reading being taken after a short time before all the gas dislodged from the film surface. Another reason could be the slow recovery of the film resistance due to lack of a sharp on-off cycle of the gas supply, the residual LPG impedes the recovery of the film. In all the four samples, the thin film interacted non-reactively with the gas at room temperature and had favourable response time as they achieved 90% recovery in the allocated time (5 – 15 minutes after exposure). The ability to recover is reliable and can be effectively used as a gas sensing surface.

5.5 The Sensitivity of TiO_2 Thin Films to LPG

The change in the sheet resistivity is a factor of sensitivity as given in *Eqn. (3.18)*. The sensitivity of the TiO_2 thin films was calculated from the resistivity measurements and related to the film thickness and displayed in Fig. 5.6.

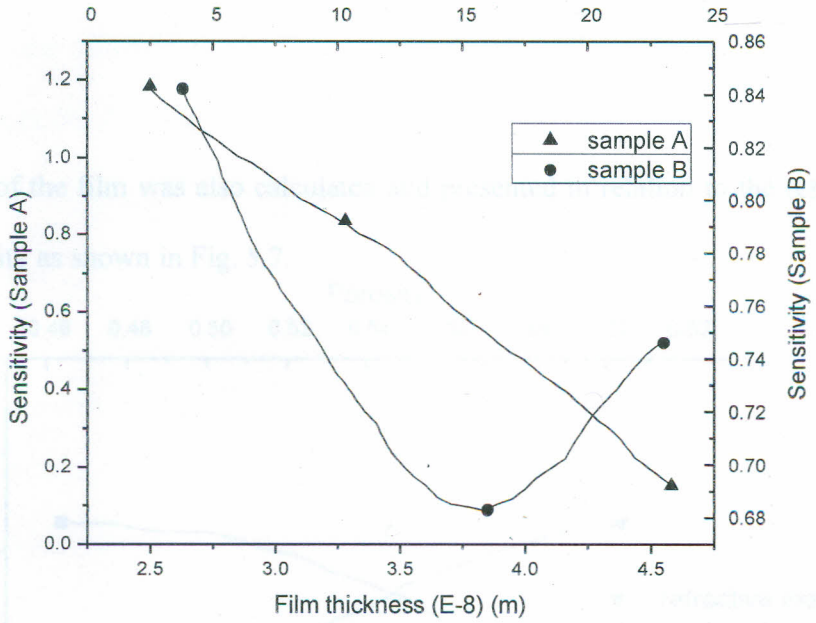

Fig. 5.6: The sensitivity of TiO_2 thin film samples A and B in relation to the film thickness for samples A and B prepared under different chamber pressures.

The two sets of samples A and B prepared at different base pressures experienced a decrease in sensitivity with increasing film thickness as the only variable. Sample A had a linear response while B samples had an increasing trend beyond 15 nm thickness. From XRF analysis, the amount of TiO_2 in the film was observed to increase with film thickness, since TiO_2 is a semiconductor, the trend observed in Fig. 5.6 suggests that

conduction results from the grain boundaries as the potential barrier increases with the increase in the amount of TiO_2 being deposited. However increasing trend observed in sample B could not be explained within the scope of this study. Other studies carried out by Zhou *et al* [25] showed that the grain size increases with the film thickness which was further related to the crystalline phases of TiO_2 as observed by Mabrook and Hawkins [11].

The sensitivity of the film was also calculated and presented in relation to the refractive index and porosity as shown in Fig. 5.7.

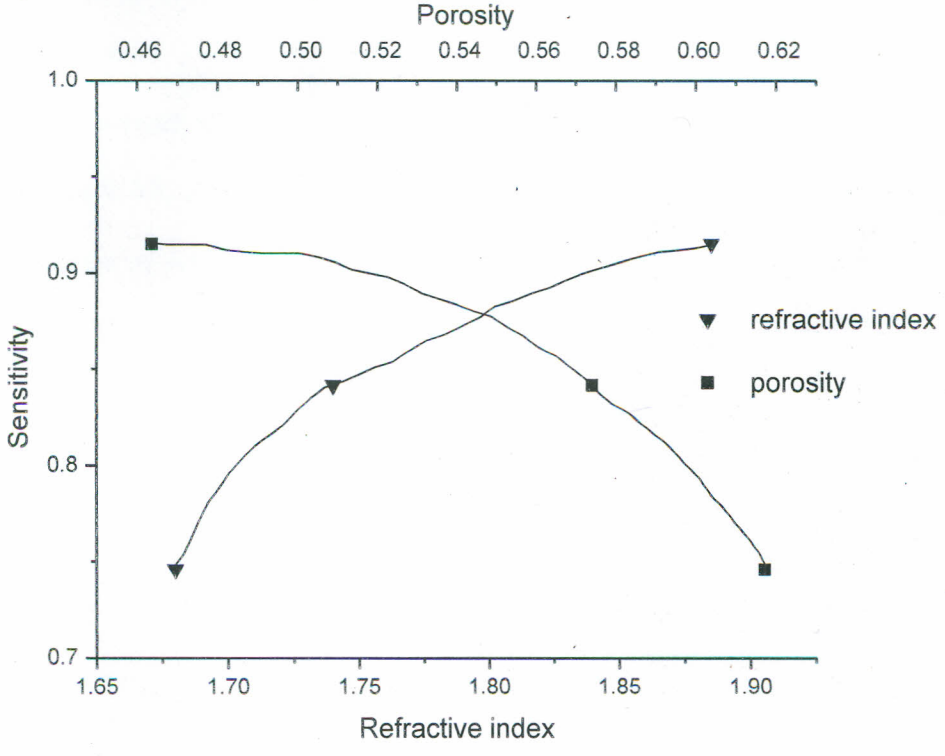

Fig. 5.7: the sensitivity of TiO_2 thin film in relation to refractive index and porosity

The film sensitivity improved as the refractive index increased but dropped with increasing porosity. Since porosity is a function of the refractive index from Eqn. 3.17, it describes the quality of the film in terms of the packing density. The high sensitivity for the highly porous films could be explained by high adsorption of LPG at the grain boundaries as opposed to the crystal sites of the TiO_2 surface. The results in Fig. 5.7 are consistent with the results obtained for sensitivity TiO_2 films prepared by other deposition methods like DC magnetron sputtering [18, 25, 38].

CHAPTER SIX

CONCLUSIONS AND SUGGESTIONS FOR FURTHER RESEARCH

6.0 Summary

Thin films of TiO_2 prepared by thermal evaporation are observed to be sensitive to LPG gas. The sensitivity is deduced from sheet resistivity measurements before, during and after exposure to the test gas. The sensitivity of the film is affected by the film thickness, the refractive index and the film porosity as dictated by the conditions of the film preparations.

6.1 Conclusions

The refractive indices of the films were calculated from the transmittance spectra measured using SP320. The films prepared at a lower chamber pressure, 6.0×10^{-5} mbar, had higher values of refractive indices between 1.73 – 1.88 compared to indices in the range of 1.67 – 1.78 for samples prepared at a higher chamber pressure, 1.0×10^{-4} mbar. This was attributed to the increase in packing density of the films as the films got optically denser when prepared under low chamber pressure.

The sheet resistivity measured on the two sets of samples A and B was found to be a function of both chamber pressure and the film thickness. Samples prepared at a low pressure (6.0×10^{-5} mbar) exhibited resistivity in the range of 2.3 kΩ to 2.97 kΩ, while samples prepared at 1.0×10^{-4} mbar had values of their resistivity between 1.91 kΩ and 3.43 kΩ before exposure to the test gas. During exposure to the test gas, both sets of samples showed a decline in sheet resistivity. The resistivity drop ranged between

0.009 kΩ and 0.04 kΩ, with the main variable being the sample thickness. The drop in resistance and recovery of the films after exposure to LPG implies that LPG molecules interacted weakly and reversibly with TiO_2 films.

Thicker samples had a lower sensitivity deviation than thinner samples, hence thinner samples should be considered when fabricating gas sensors with improved sensitivity. The improved response of the thinner films over thicker films shows that conduction mainly occurs at the pore phase rather than at the solid phase since the XRF analysis showed higher percentage of TiO_2 present in the thicker films.

Samples prepared in both environments, A and B, showed a recovery of about 90% of the resistivity value after the samples were removed from an LPG rich environment. This shows a reversible interaction of the film with the test gas, a trend supporting the better performance of the thinner film over the thicker film.

The refractive index of TiO_2 thin film deposited by thermal evaporation increased with decrease in chamber pressure. Low chamber pressure allowed for the formation of denser films as the packing density increased with low pressure in the chamber. The films with higher refractive index exhibited higher ranges of sheet resistivity than those with lower refractive index. However, the change in resistivity due to the influence of LPG was observed in all the films. Film thickness is a significant variable to consider when analysing the sheet resistivity changes. Thinner films tended to exhibit larger resistance

deviations compared to thicker films when exposed to LPG. This makes TiO_2 thinner films more viable for better sensitivity to LPG.

6.2 Suggestions for Further Research

This study focused its analysis on as-deposited TiO_2 thin film. The effect of post-deposition treatment (e.g. thermal annealing) of thin film is a significant factor that can be further investigated to fully understand optimization of the sensitivity and stability of the TiO_2 sensor surface.

For a continuous collection of data, a computer program like LabVIEW can be used to interface the sensing mechanism and the data storage device. The continuous data would be used to estimate response time of the sensing surface which is a vital in fabricating gas sensors.

Thin film surface characterization such as scanning electron microscopy (SEM) can be done on the TiO_2 thin films prepared in this study to help understand the coarseness or smoothness of the surfaces as this directly affects the adsorption and desorption process in gas sensing.

REFERENCES

[1]. Gibilisco S. The illustrated dictionary of electronics 6th edition, Tab books, McGraw-Hill, Toronto. 581 (1994)

[2]. Obida M., Afify H., Abou M. and Zaid H. Nanocrystalline anatase titania thin films synthesized by spray pyrolysis for gas detection. *Egypt J. Solids*. Vol. 28 No. 1, 35-50 (2005)

[3]. Trimboli J. The development and characterization of titania based gas sensors for combustion process monitoring, PhD thesis, Ohio state university. USA. (2005)

[4]. Dang T., Dang D., Nguyen D., Nguyen H., and Nguyen C. Preparation and characterization of nanostructured TiO_2 & SnO_2. Proceedings of the 8th German-Vietnamese seminar on physics and engineering. Erlangen (2005).

[5]. Licznerski B. Thick film gas microsensors based on tin dioxide. Bulletin of the *Polish Academy of Technical Sciences*. Vol. 52 No. 1, 37-42 (2004).

[6]. Kirk-Othmer., Encyclopaedia of Chemical Technology, vol. 23, 3rd edition, John Wiley & Sons, New York (1983).

[7]. Fujishimo A., Hashimoto K. and Wanabe T. (1999). TiO_2 Photocatalysis, Fundamentals and Applications, BKC Inc, Tokyo Japan (1999).

[8]. Jakubik W. Investigations of thin film of titanium dioxide in a surface acoustic wave gas sensor system. *Molecular and quantum acoustics*. Vol. 27, 133-139 (2006).

[9]. Miguel J. A. Thin films for Gas Sensors, PhD thesis, departamento de Fisica, Universidade do Minho. Spain (2003).

[10]. Sathyamoorthy R., Sudhagar P., Chandramohan S. and Vijayakumar K. Photoelectrical properties of crystalline titanium dioxide thin films after thermo-annealing, *Cryst. Res. Technol.* 42, No. 5, 498 – 503 (2007).

[11]. Mabrook M. & Hawkin P. Benzene sensing using thin film of TiO_2 operating at room temperature. *Sensors 2*, 374-382 (2002).

[12]. Health Council of the Netherlands. LPG health based reassessment of administrative occupational exposure limits (2004).

[13]. Capone S., Forleo A., Francioso L., Rella R., Siciliano P., Spadavecchia J., Presicce D. and Taurino M. Solid state gas sensors: state of the art and future activities. *Journal of Optoelectronics and Advanced Materials*. Vol 5, No. 5. 1335-1348 (2003).

[14]. Dunne J. World liquefied petroleum gas association. Guidelines for good safety practices in LP Gas industry. Supported by United Nations Environment Programme. 10-33 (2008).

[15]. Ohring M. The Materials Science of Thin Films. Stevens Insitute of Technology, New Jersey. Academic Press 49-544, (2001).

[16]. Castillo N. Olguin D. and Conde-Gallardo A. (2004). Structural and morphological properties of TiO_2 thin film.

[17]. Ray A., Tracey S., McQuillin B. and Hodgson S. Optical studies on sol-gel derived titanium dioxide films. *IEE proceedings-science measurement technology*. Vol. 147, No. 6, 301-304 (2000).

[18]. Mechiakh R. and Bensaha R. Analysis of optical and structural properties of sol-gel TiO_2 thin films. *Moroccan Statistical Physical Society*. Vol 7, No.1, 54-57 (2006).

[19]. Kozlowska K., Lukowiak A., Szczurek A., Dudek K. and Maruszewski K. Sol-gel coatings for electrical gas sensors. *Optica applicata.* Vol XXXV, No. 4. 783-790 (2005).

[20]. Bernadi M., Lee E., Lisboa-Filho P., Leite E., Longo E. and Vanela J. TiO_2 thin film growth using the MOCVD method. *Materials Research.* Vol 4 No. 3. 223-226 (2001).

[21]. Dutta K., Marla F., Hunter G. and George M. Reactively sputtered titania films as high temperature carbon monoxide sensor, *Sensors and Actuators B 106.* 810-815 (2005).

[22]. Dakka A., Lafait J. Abd-Lefdil and Sella H. Optical study of titanium dioxide thin films prepared by RF sputtering. *Moroccan Stat. Phy. Society.* Vol. 2, No. 2. 114-119 (1999).

[23]. Hassan M., Haseeb A., Saidur R. and Masjuki H. Effects of annealing treatment on optical properties of anatase TiO_2 thin films. Proceedings of World Academy of Science, Engineering & Technology. Vol 30. 221-225 (2008).

[24]. Karunagaran B., Kumar R., Viswanathan C., Mangalaraj D., Narayandass K. and Rao G. Optical constants of DC magnetron sputtered TiO_2 thin films measured by spectroscopic ellipsometry. *Crystal Research Technology, 38,* No. 9. 773-778 (2003).

[25]. Zhou W., Xiaoxia Z., Xiaochen W., Luqi Y., Qiwei S. and Yuxing X. Structural and optical properties of TiO_2 thin films deposited by reactive dc magnetron sputtering. *Journal of Korean Physical Society.* Vol. 49, No. 5, 2168-2175 (2006).

[26]. Waita S., Aduda B., Mwabora J., Granquist C., Lindqvist S., Niklasson G., Hagfeldt A. and Boschloo G. Electron transport & recombination in dye sensitised solar cells fabricated from obliquely sputter deposited & thermally annealed TiO_2 films. *Journal of Electranalytical chemistry* 605, 151-156 (2007).

[27]. Stamate M., Lazar G. & Lazar I. Anatase-Rutile TiO_2 thin film deposited in a D.C. magnetron sputtering system. *Romanian Journal of Physics*. Vol 53 No. 1-2, 217-221 (2008).

[28]. Brien V., Dauscher A., Weber S., Ledevil J. and Machizaud F. Structural & chemical investigation of thermally evaporated Ti-Ni-Zr films. *Bulg. J. Phys.* 29 (2002) 142-150

[29]. Chong L., Mallik K., Groot C. and Kersting R. The structural and electrical properties of thermally grown TiO_2 thin films. *J. Phys, Condens. Matter* 18 (2006) 645-657

[30]. Figaro engineering Inc. www.figaro.co.jp (Jan 2010).

[31]. Comini E., Faglia G. and Sberveglieri G. Stable and highly sensisitve gas sensors based on semiconducting oxide nanobelts, *Appl. Phy. Letters*. Vol. 81 No. 10, 1869-1871 (2002).

[32]. Toan W., Giang H., Hieu N., and Thu D. Sensor based on nano-crystalline perovskite oxides. Proceedings of 9th Asia Pacific Physics Conference, Hanoi Vietnam (2004).

[33]. Comini E. and Sberveglieri G. Gas-sensing characterization of TiO_2-ZnO based thin film. *IEEE sensors exco*, Daegu, Korea. 964-967 (2006).

[34]. Laszlo B., Smulko J., Heszler P. and Granqvist C. The sensitivity, selectivity, sensor information and optical size of resistive chemical sensors. *Nanotechnology perceptions*. Vol. 3. 1-11 (2007).

[35]. Shobi B. Gas sensor – studies on sensor film deposition, ASIC design & testing. MSc thesis. Indian Institute of Sciences, Bangalore – 560012, India (2007).

[36]. Ferrari E., Ridi A. and Muselli M. Modeling and interpretation of responses from e-noses in the detection of gases in air, *CNR- IEIIT* via De Marini, Italy.

[37]. Kenya Gazette Supplement No. 50. Legislative supplement No. 31. Special issue. Government printer, Nairobi. 436-449 (2009).

[38]. Rao N. Influence of deposition parameters on optical properties of TiO_2 films. *Society of Photo-optical Instrumentation Engineers* 41(9), 2357-2364 (2002).

[39]. Oduor A. O. Electrical transport properties in evaporated cadmium selenide thin films, PhD thesis, Dept. of Physics, University of Keele (1997).

[40]. Amptek Inc., X-ray diffraction, Bedford, MA 01730-2204, USA.

[41]. Morton D. E. Preparation and properties of optical thin film materials, copyrighted notes for a course prepared for the Society of Vacuum Coaters Education Program, 1-13 (2001).

[42]. Stockett M. Optical properties of thin transparent conducting oxide films on glass for photovoltaic application. PhD thesis, Ohio State University. USA. (2006).

[43]. Keithley Instruments. User's manual, 7th printing, Cleveland, Ohio USA, 73-143 (1998).

[44]. William B. R. Coatings: An Introduction to the Cleaning Procedures, Sol-Gel Gateway tutorial (2003).

[45]. Edwards. Instruction manual for Auto 306 Vacuum Coater with turbomolecular pumping system, E090-03-860 issue E (1996).

[46]. Popov Alexey. TiO_2 nanoparticles as UV protectors in skin. PhD thesis, Faculty of Technology. University of Oulu. Finland (2008).

[47]. Sankar S. and Gopchandran K. Effect of growth parameters on structural, electrical and optical properties of titanium oxide thin films. *Indian Journal of Pure and Applied Physics*. Vol. 46, 791-796 (2008).